

## Synthesis and Photovoltaic Properties of New Metalloporphyrin-Containing Polyplatinyne Polymers

Hongmei Zhan,<sup>†</sup> Simon Lamare,<sup>‡</sup> Annie Ng,<sup>§</sup> Tommy Kenny,<sup>‡</sup> Hannah Guernon,<sup>‡</sup> Wai-Kin Chan,<sup>¶</sup> Aleksandra B. Djurišić,<sup>\*,§</sup> Pierre D. Harvey,<sup>\*,‡</sup> and Wai-Yeung Wong<sup>\*,†</sup>

<sup>†</sup>Institute of Molecular Functional Materials (Areas of Excellence Scheme, University Grants Committee, Hong Kong) and Department of Chemistry and Centre for Advanced Luminescence Materials, Hong Kong Baptist University, Kowloon Tong, Kowloon, Hong Kong, P.R. China

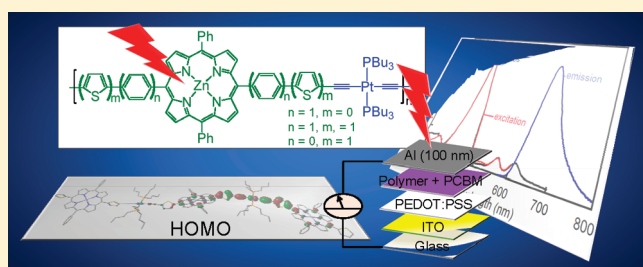
<sup>‡</sup>Département de Chimie, Université de Sherbrooke, 2550 Boul. Université, Sherbrooke, PQ, J1K 2R1 Canada

<sup>§</sup>Department of Physics, The University of Hong Kong, Pokfulam Road, Hong Kong, P.R. China

<sup>¶</sup>Department of Chemistry, The University of Hong Kong, Pokfulam Road, Hong Kong, P.R. China

Supporting Information

**ABSTRACT:** Three new solution-processable platinum(II) polyyne polymers containing zinc(II) porphyrinate chromophores **P1**, **P2**, and **P3** and their corresponding dinuclear model complexes were synthesized via the CuI-catalyzed dehydrohalogenation reaction of the platinum(II) chloride precursor and each of the respective bis(ethynyl)-zinc(porphyrin) metalloligands. The thermal, photophysical (absorption, excitation and emission spectra), electrochemical, and photovoltaic properties of **P1**–**P3** were investigated. These results are also correlated by time-dependent density functional theory (TDDFT) calculations. The computations corroborate the presence of moderate conjugation in the  $\pi$ -systems, somewhat more accentuated for **P3** where more favorable dihedral angles between the porphyrin and thiophene rings are noted. Moreover, the computed excited states are predicted to be  $\pi-\pi^*$  in nature with some charge transfer components from the *trans*-[ $-\text{C}\equiv\text{CPt}(\text{L})_2\text{C}\equiv\text{C}-$ ]<sub>n</sub> unit to the porphyrin rings. The optical bandgaps range from 1.93 to 2.02 eV for **P1**–**P3**. Intense  $\pi-\pi^*$ -localized fluorescence emissions typical of the Q-bands of the polymers were observed. The effect of thiophene ring along the polymer chain on the extent of  $\pi$ -conjugation, luminescent and photovoltaic properties of these metalated materials was also examined. Bulk heterojunction solar cells using these metallopolymers as an electron donor blended with a methanofullerene electron acceptor were studied. In one case, the metallopolymer **P3** showed a power conversion efficiency of 1.04% with the open-circuit voltage of 0.77 V, short-circuit current density of 3.42 mA cm<sup>-2</sup> and fill factor of 0.39 under illumination of an AM 1.5 solar cell simulator.



### INTRODUCTION

Organic solar cells have attracted much attention in recent years owing to their advantages of low-cost fabrication by solution processing and easy chemical tailoring, as well as potential applications in flexible, lightweight and large-area energy-harvesting devices. Bulk heterojunction devices fabricated by simply blending organic donor materials and methanofullerene acceptor materials, such as [6,6]-phenyl C<sub>61</sub>-butyric acid methyl ester (PCBM), in the same organic solvents has become one of the most successful device architectures developed in this field, which result in the efficient photoinduced electron transfer from donor materials to fullerene derivatives.<sup>1</sup> Most of the efforts have been focused on developing novel donor materials with sufficient solubility, low optical band gap and high hole mobility, which would lead to efficient solar cells.

Porphyrins contain an extensively conjugated two-dimensional  $\pi$ -system which renders them suitable for light-harvesting and efficient electron transfer because the uptake or release of

electrons results in minimal structural change.<sup>2</sup> Porphyrin has rich and extensive optical absorption in the visible spectrum and high mobility.<sup>3–5</sup> The typical absorption spectra of porphyrin units exhibit sharp and strong Soret bands (410–430 nm) and weak Q-bands (530–540 nm) without absorption features between them. In addition, efficient photoinduced electron separation and transfer between porphyrins and fullerene derivatives have also been reported.<sup>6–8</sup> Therefore, organic solar cells using porphyrin-containing molecules,<sup>9–11</sup> oligomers,<sup>12</sup> and polymers<sup>13–15</sup> as photoactive layers have been extensively investigated in recent years. Unfortunately, only low power conversion efficiencies (PCEs) were obtained so far. For example, the PCEs of the devices based on porphyrin triad,<sup>9</sup> liquid-crystalline porphyrin,<sup>4</sup> porphyrin dendrimer,<sup>10</sup> porphyrin-containing oligomers,<sup>12</sup> and main-chain

Received: March 17, 2011

Revised: May 22, 2011

Published: June 13, 2011

porphyrin polymers<sup>14</sup> are only 0.035%, 0.775%, 0.32%, 0.000081% and 0.3%, respectively. More recently, new advances have been realized using supramolecular and nanocomposite systems. Novel organic photovoltaic systems using supramolecular complexes of porphyrin-peptide oligomers with fullerene clusters assembled as three-dimensional arrays onto SnO<sub>2</sub> films have been constructed with the PCE reaching 1.6%<sup>16</sup> whereas photovoltaic cells using composite nanoclusters of porphyrins and fullerenes with gold nanoparticles were also developed to afford a PCE of 1.5%.<sup>3</sup>

On the other hand, platinum metallocopolyne polymers of the form *trans*-[−Pt(L)<sub>2</sub>C≡CRC≡C−]<sub>n</sub> (L is an auxiliary phosphine ligand, and R is an aromatic spacer unit) have attracted a great deal of research attention. The interest derives from the fact that incorporation of platinum into the conjugated polymers can result in good overlap between the d-orbital of Pt with the p-orbital of the alkyne unit, and so the two alkyne units can mutually interact through the Pt d<sub>xy</sub> and d<sub>yz</sub> orbitals, which lead to efficient electronic π-conjugation and delocalization along the polymer chain.<sup>17</sup> Moreover, due to strong spin–orbit coupling resulting from the presence of platinum, intersystem crossing is enhanced which enables the spin-forbidden triplet emission to become partially allowed,<sup>18–24</sup> and can extend the exciton diffusion length. These features enable platinum-containing metallocopolyne polymers more feasible to be used as the donor materials in photovoltaic cells, and encouraging progress has been made in recent years.<sup>25–28</sup>

In view of the considerations above, the use of metallocoporphyrins as the building block in combination with linear conjugated systems of transition metal-alkyne polymers for the design of new p-type photovoltaic active materials serves as a good illustration of the recent trend toward solution-processable functional polymers. We present here the synthesis, characterization and theoretical modeling studies of several platinum polyyne polymers coupled with zinc(II) porphyrinate chromophores, and their photovoltaic properties have been investigated. The introduction of thiophene unit into the porphyrin-based polymer main chain is expected to extend the π-conjugation and cover the missing absorption region (430–530 nm) or enhance the absorption of the weaker Q-bands. Phenyl rings at positions 10 and 20 of the zinc porphyrin ring are used for enhancing the molecular ordering, hence improving the interpenetrating network with the fullerene derivative. This work represents the first example of porphyrin-containing polymetallaynes used for harvesting solar energy in solution-processed photovoltaic devices.

## EXPERIMENTAL SECTION

**Materials.** All reactions were carried out under a nitrogen atmosphere by using standard Schlenk techniques. Solvents were dried and distilled from appropriate drying agents under an inert atmosphere prior to use. Glassware was oven-dried at about 120 °C. All reagents and chemicals, unless otherwise stated, were purchased from commercial sources and used without further purification. 5-Bromothiophene-2-carbaldehyde<sup>29</sup> and *meso*-phenyldipyrromethane<sup>30</sup> *trans*-[PtCl(Ph)-(PEt<sub>3</sub>)<sub>2</sub>]<sup>31</sup> and *trans*-[Pt(PBu<sub>3</sub>)<sub>2</sub>Cl]<sup>32</sup> were prepared according to the literature methods. All reactions were monitored by thin-layer chromatography (TLC) with Merck precoated glass plates. Flash column chromatography and preparative TLC were carried out using silica gel from Merck (230–400 mesh).

**Syntheses.** The syntheses of all the ligand precursors are given in the Supporting Information.

**General Synthetic Procedures of Porphyrin Compounds.**<sup>14</sup> *5,15-Bis(1,4-trimethylsilylethyanylbenzene)-10,20-bis(phenyl)porphyrin (L1H-TMS).* A solution of 4-(2-(trimethylsilyl)ethynyl)benzaldehyde (119 mg, 0.59 mmol) and *meso*-phenyldipyrromethane (139 mg, 0.59 mmol) in CH<sub>2</sub>Cl<sub>2</sub> (60 mL) was purged with nitrogen for 30 min, and then trifluoroacetic acid (TFA) (47 mg, 0.41 mmol) was added. The mixture was stirred for 3 h at room temperature, and then 2,3-dichloro-5,6-dicyano-1,4-benzoquinone (DDQ) (267 mg, 1.2 mmol) was added. After the mixture was stirred at room temperature for an additional 30 min, the reaction was quenched by adding triethylamine (0.6 mL). The solvent was removed, and the residue was purified by flash column chromatography on silica gel using CH<sub>2</sub>Cl<sub>2</sub>/hexane (1:1, v/v) as the eluent. Recrystallization from CH<sub>2</sub>Cl<sub>2</sub>/methanol gave L1H-TMS as a purple solid (45 mg, 11%).  $\nu(C\equiv C)$  2153 cm<sup>−1</sup>. <sup>1</sup>H NMR (CDCl<sub>3</sub>, 400 MHz, δ): 8.86 (d, *J* = 5.2 Hz, 4H, Ar), 8.81 (d, *J* = 5.0 Hz, 4H, Ar), 8.21–8.19 (m, 4H, Ar), 8.18–8.15 (m, 4H, Ar), 7.86 (d, *J* = 8.1 Hz, 4H, Ar), 7.78–7.74 (m, 6H, Ar), 0.38 (s, 18H, TMS), −2.82 (s, 2H, NH) ppm. FAB-MS: *m/z* 807.5 (M<sup>+</sup>).

The same procedures were applied to prepare L2H-TMS and L3H-TMS from their corresponding aromatic aldehyde derivatives and *meso*-phenyldipyrromethane.

*5,15-Bis(1,4-(2,5-trimethylsilylethyanylthienyl)benzene)-10,20-bis(phenyl)porphyrin (L2H-TMS).* Purple solid, yield: 10%.  $\nu(C\equiv C)$  2141 cm<sup>−1</sup>. <sup>1</sup>H NMR (CDCl<sub>3</sub>, 400 MHz, δ): 8.91–8.89 (m, 4H, Ar), 8.87–8.85 (m, 4H, Ar), 8.21 (d, *J* = 7.8 Hz, 8H, Ar), 7.94 (d, *J* = 7.9 Hz, 4H, Ar), 7.77–7.74 (m, 6H, Ar), 7.45 (d, *J* = 3.7 Hz, 2H, Ar), 7.35 (d, *J* = 3.7 Hz, 2H, Ar), 0.31 (s, 18H, TMS), −2.76 (s, 2H, NH) ppm. FAB-MS: *m/z* 971.5 (M<sup>+</sup>).

*5,15-Bis(2,5-trimethylsilylethyanylthiophene)-10,20-bis(phenyl)porphyrin (L3H-TMS).* Purple solid, yield: 14%.  $\nu(C\equiv C)$  2144 cm<sup>−1</sup>. <sup>1</sup>H NMR (CDCl<sub>3</sub>, 400 MHz, δ): 9.06 (d, *J* = 4.7 Hz, 4H, Ar), 8.84 (d, *J* = 4.7 Hz, 4H, Ar), 8.20–8.19 (m, 4H, Ar), 7.81–7.77 (m, 6H, Ar), 7.75 (d, *J* = 3.6 Hz, 2H, Ar), 7.64 (d, *J* = 3.6 Hz, 2H, Ar), 0.35 (s, 18H, TMS), −2.76 (s, 2H, NH) ppm. FAB-MS: *m/z* 819.4 (M<sup>+</sup>).

**General Synthetic Procedures of Zn–Porphyrin Complexes.** Zinc(II) *5,15-Bis(1,4-trimethylsilylethyanylbenzene)-10,20-bis(phenyl)porphyrin (L1-TMS).* To a solution of L1H-TMS (41 mg, 0.05 mmol) in CH<sub>2</sub>Cl<sub>2</sub> (16 mL) was added a solution of Zn(OAc)<sub>2</sub>·H<sub>2</sub>O (25 mg, 0.11 mmol) in methanol (1 mL). The reaction mixture was stirred at room temperature for 5 h. Evaporation of the solvent and purification by column chromatography using CH<sub>2</sub>Cl<sub>2</sub>/hexane (1:1, v/v) as the eluent afforded the product L1-TMS (44 mg, 98%) as a purple solid.  $\nu(C\equiv C)$  2156 cm<sup>−1</sup>. <sup>1</sup>H NMR (CDCl<sub>3</sub>, 400 MHz, δ): 8.97 (d, *J* = 4.8 Hz, 4H, Ar), 8.91 (d, *J* = 4.8 Hz, 4H, Ar), 8.22–8.19 (m, 4H, Ar), 8.17–8.15 (m, 4H, Ar), 7.87 (d, *J* = 8.0 Hz, 4H, Ar), 7.77–7.75 (m, 6H, Ar), 0.38 (s, 18H, TMS) ppm. <sup>13</sup>C NMR (CDCl<sub>3</sub>, 125 MHz, δ): 150.21, 149.81, 143.03, 142.56, 134.29, 134.19, 132.18, 131.67, 130.15, 128.82, 127.51, 126.51, 121.31, 120.27 (Ar), 105.02, 95.32 (C≡C), 0.09 (TMS) ppm. FAB-MS: *m/z* 869.4 (M<sup>+</sup>).

The same procedures were used to prepare L2-TMS and L3-TMS from their corresponding starting materials L2H-TMS and L3H-TMS.

Zinc(II) *5,15-Bis(1,4-(2,5-trimethylsilylethyanylthienyl)benzene)-10,20-bis(phenyl)porphyrin (L2-TMS).* Purple solid, yield: 93%.  $\nu(C\equiv C)$  2142 cm<sup>−1</sup>. <sup>1</sup>H NMR (CDCl<sub>3</sub>, 400 MHz, δ): 9.02 (m, 4H, Ar), 8.97–8.95 (m, 4H, Ar), 8.24–8.21 (m, 8H, Ar), 7.95 (d, *J* = 7.9 Hz, 4H, Ar), 7.79–7.73 (m, 6H, Ar), 7.45 (d, *J* = 3.8 Hz, 2H, Ar), 7.35 (d, *J* = 3.8 Hz, 2H, Ar), 0.32 (s, 18H, TMS) ppm. <sup>13</sup>C NMR (CDCl<sub>3</sub>, 125 MHz, δ): 150.36, 150.12, 145.70, 142.76, 135.11, 134.49, 134.10, 132.96, 132.28, 131.87, 128.96, 127.61, 126.66, 124.10, 123.38, 122.77, 121.43, 120.47 (Ar), 99.99, 97.82 (C≡C), 0.09 (TMS) ppm. FAB-MS: *m/z* 1033.4 (M<sup>+</sup>).

Zinc(II) *5,15-Bis(2,5-trimethylsilylethyanylthiophene)-10,20-bis(phenyl)porphyrin (L3-TMS).* Purple solid, yield: 96%.  $\nu(C\equiv C)$  2145 cm<sup>−1</sup>. <sup>1</sup>H NMR (CDCl<sub>3</sub>, 400 MHz, δ): 9.16 (d, *J* = 4.7 Hz, 4H, Ar), 8.94 (d, *J* = 4.7 Hz, 4H, Ar), 8.21–8.19 (m, 4H, Ar), 7.80–7.76 (m, 6H, Ar), 7.74

(d,  $J = 3.6$  Hz, 2H, Ar), 7.64 (d,  $J = 3.6$  Hz, 2H, Ar), 0.35 (s, 18H, TMS) ppm.  $^{13}\text{C}$  NMR ( $\text{CDCl}_3$ , 125 MHz,  $\delta$ ): 150.81, 150.61, 145.51, 142.43, 134.43, 133.27, 132.56, 131.90, 131.80, 127.74, 126.69, 125.18, 122.11, 111.47 (Ar), 99.92, 97.61 (C≡C) ppm. FAB-MS:  $m/z$  881.2 ( $\text{M}^+$ ).

**Synthesis of Zn(II) Porphyrinate Ligands.** The ligands were synthesized by deprotection reaction of L1-TMS to L3-TMS using tetrabutylammonium fluoride (TBAF) as a base in THF. A typical example was given for L1.

**Zinc(II) 5,15-Bis(1,4-ethynylbenzene)-10,20-bis(phenyl)porphyrin (L1).** TBAF (0.13 mL, 1 M in THF) was added to a stirred solution of L1-TMS (54 mg, 0.06 mmol) in THF (8 mL). After stirring for 5 min, water (30 mL) was added to quench the reaction. The solution was extracted with chloroform, washed with water and dried over anhydrous  $\text{MgSO}_4$ . After evaporation of the solvent, the residue was purified by column chromatography using  $\text{CH}_2\text{Cl}_2$ /hexane (1.2:1, v/v) as the eluent to give L1 (41 mg, 90%) as a purple solid. IR (KBr):  $\nu(\text{C}\equiv\text{C})$  2106  $\text{cm}^{-1}$ .  $^1\text{H}$  NMR ( $\text{CDCl}_3$ , 400 MHz,  $\delta$ ): 8.97–8.95 (m, 4H, Ar), 8.93 (m, 4H, Ar), 8.22–8.17 (m, 8H, Ar), 7.88 (d,  $J = 7.8$  Hz, 4H, Ar), 7.77–7.74 (m, 6H, Ar), 3.31 (s, 2H, C≡CH) ppm.  $^{13}\text{C}$  NMR ( $\text{CDCl}_3$ , 125 MHz,  $\delta$ ): 150.29, 149.83, 143.44, 142.62, 134.40, 134.32, 132.29, 132.06, 131.63, 130.08, 127.59, 126.59, 121.41, 120.18 (Ar), 83.73, 78.16 (C≡C) ppm. FAB-MS:  $m/z$  725.0 ( $\text{M}^+$ ). Anal. Calcd for  $\text{C}_{48}\text{H}_{28}\text{N}_4\text{Zn}$ : C, 79.39; H, 3.89; N, 7.72. Found: C, 79.21; H, 4.05; N, 7.57.

**Zinc(II) 5,15-Bis(1,4-(2,5-ethynylthienyl)benzene)-10,20-bis(phenyl)porphyrin (L2).** Purple solid, yield: 85%. IR (KBr):  $\nu(\text{C}\equiv\text{C})$  2098  $\text{cm}^{-1}$ .  $^1\text{H}$  NMR ( $\text{CDCl}_3$ , 400 MHz,  $\delta$ ): 9.02–9.00 (m, 4H, Ar), 8.98–8.95 (m, 4H, Ar), 8.25–8.22 (m, 8H, Ar), 7.97 (d,  $J = 8.1$  Hz, 4H, Ar), 7.77 (m, 6H, Ar), 7.48 (d,  $J = 3.8$  Hz, 2H, Ar), 7.41 (d,  $J = 3.7$  Hz, 2H, Ar), 3.49 (s, 2H, C≡CH) ppm.  $^{13}\text{C}$  NMR ( $\text{CDCl}_3$ , 125 MHz,  $\delta$ ): 145.56, 142.18, 142.12, 141.98, 135.27, 134.63, 134.11, 133.16, 127.86, 127.82, 126.80, 126.78, 124.22, 123.47, 122.85, 120.44, 120.32, 119.47 (Ar), 100.07, 97.78 (C≡C) ppm. FAB-MS:  $m/z$  889.4 ( $\text{M}^+$ ). Anal. Calcd for  $\text{C}_{56}\text{H}_{32}\text{N}_4\text{S}_2\text{Zn}$ : C, 75.54; H, 3.62; N, 6.29. Found: C, 75.34; H, 3.79; N, 6.42.

**Zinc(II) 5,15-Bis(2,5-ethynylthiophene)-10,20-bis(phenyl)porphyrin (L3).** Purple solid, yield: 87%.  $\nu(\text{C}\equiv\text{C})$  2101  $\text{cm}^{-1}$ .  $^1\text{H}$  NMR ( $\text{CDCl}_3$ , 400 MHz,  $\delta$ ): 9.17 (d,  $J = 4.7$  Hz, 4H, Ar), 8.96 (d,  $J = 4.7$  Hz, 4H, Ar), 8.21–8.19 (m, 4H, Ar), 7.79–7.77 (m, 8H, Ar), 7.68 (d,  $J = 3.6$  Hz, 2H, Ar), 3.57 (s, 2H, C≡CH) ppm.  $^{13}\text{C}$  NMR ( $\text{CDCl}_3$ , 125 MHz,  $\delta$ ): 150.75, 150.61, 145.75, 142.36, 134.38, 133.11, 132.58, 132.22, 131.74, 127.72, 126.66, 123.99, 122.13, 111.26 (Ar), 82.13, 77.10 (C≡C) ppm. FAB-MS:  $m/z$  737.2 ( $\text{M}^+$ ). Anal. Calcd for  $\text{C}_{44}\text{H}_{24}\text{N}_4\text{S}_2\text{Zn}$ : C, 71.59; H, 3.28; N, 7.59. Found: C, 71.68; H, 3.50; N, 7.45.

**Synthesis of Platinum Polyne Polymers (P1–P3).** The polymers were prepared by the dehydrohalogenative polycondensation between *trans*-[Pt(PBu<sub>3</sub>)<sub>2</sub>Cl<sub>2</sub>] and each of the ligands (L1–L3). A typical procedure was given for P1 starting from L1.

Polymerization was carried out by mixing L1 (30 mg, 0.04 mmol), *trans*-[Pt(PBu<sub>3</sub>)<sub>2</sub>Cl<sub>2</sub>] (28 mg, 0.04 mmol) and CuI (3.00 mg) in Et<sub>3</sub>N/CH<sub>2</sub>Cl<sub>2</sub> (12 mL, 1:1, v/v). After stirring at room temperature for 24 h under nitrogen, the solution mixture was evaporated to dryness. The residue was redissolved in CH<sub>2</sub>Cl<sub>2</sub> and filtered through a short alumina column using the same eluent to remove ionic impurities and catalyst residues. After removal of the solvent, the crude product was purified by precipitation in CH<sub>2</sub>Cl<sub>2</sub> from MeOH twice to give the polymer P1 (15 mg, 27%) as a purple solid. IR (KBr):  $\nu(\text{C}\equiv\text{C})$  2099  $\text{cm}^{-1}$ .  $^1\text{H}$  NMR ( $\text{CDCl}_3$ , 400 MHz,  $\delta$ ): 9.05–8.95 (m, 8H, Ar), 8.24–8.09 (m, 8H, Ar), 7.78–7.71 (m, 10H, Ar), 2.42–2.38 (m, 12H, PBu<sub>3</sub>), 1.70–1.58 (m, 12H, PBu<sub>3</sub>), 1.51–1.42 (m, 12H, PBu<sub>3</sub>), 0.94 (t, 18H, PBu<sub>3</sub>) ppm.  $^{31}\text{P}$  NMR ( $\text{CDCl}_3$ , 162 Hz,  $\delta$ ): 3.16 ( $^1\text{J}_{\text{P}-\text{Pt}} = 2352$  Hz) ppm. Anal. Calcd for (C<sub>72</sub>H<sub>80</sub>N<sub>4</sub>P<sub>2</sub>Pt<sub>2</sub>Zn)<sub>n</sub>: C, 65.32; H, 6.09; N, 4.23. Found: C, 65.45; H, 5.87; N, 4.10. GPC (THF):  $M_w = 22325$ ,  $M_n = 9500$ , PDI = 2.35, DP = 7.

**P2.** Purple solid, yield: 32%. IR (KBr):  $\nu(\text{C}\equiv\text{C})$  2086  $\text{cm}^{-1}$ .  $^1\text{H}$  NMR ( $\text{CDCl}_3$ , 400 MHz,  $\delta$ ): 9.05–9.03 (m, 4H, Ar), 8.98–8.95 (m, 4H, Ar), 8.22–8.20 (m, 8H, Ar), 7.95 (m, 4H, Ar), 7.78–7.76 (m, 6H, Ar),

7.44 (m, 2H, Ar), 7.00 (m, 2H, Ar), 2.24–2.22 (m, 12H, PBu<sub>3</sub>), 1.71–1.67 (m, 12H, PBu<sub>3</sub>), 1.61–1.54 (m, 12H, PBu<sub>3</sub>), 1.01 (t,  $J = 7.2$  Hz, 18H, PBu<sub>3</sub>) ppm.  $^{31}\text{P}$  NMR ( $\text{CDCl}_3$ , 162 Hz,  $\delta$ ): 3.42 ( $^1\text{J}_{\text{P}-\text{Pt}} = 2328$  Hz) ppm. Anal. Calcd for (C<sub>80</sub>H<sub>84</sub>N<sub>4</sub>P<sub>2</sub>S<sub>2</sub>Pt<sub>2</sub>Zn)<sub>n</sub>: C, 64.57; H, 5.69; N, 3.76. Found: C, 64.76; H, 5.85; N, 3.68. GPC (THF):  $M_w = 50820$ ,  $M_n = 13620$ , PDI = 3.73, DP = 9.

**P3.** Green solid, yield: 35%. IR (KBr):  $\nu(\text{C}\equiv\text{C})$  2084  $\text{cm}^{-1}$ .  $^1\text{H}$  NMR ( $\text{CDCl}_3$ , 400 MHz,  $\delta$ ): 9.30–9.25 (m, 4H, Ar), 8.93–8.88 (m, 4H, Ar), 8.21–8.19 (m, 4H, Ar), 7.82–7.66 (m, 8H, Ar), 7.26 (m, 2H, Ar), 2.29–2.18 (m, 12H, PBu<sub>3</sub>), 1.73–1.70 (m, 12H, PBu<sub>3</sub>), 1.57–1.53 (m, 12H, PBu<sub>3</sub>), 1.03–0.88 (m, 18H, PBu<sub>3</sub>) ppm.  $^{31}\text{P}$  NMR ( $\text{CDCl}_3$ , 162 Hz,  $\delta$ ): 3.30 ( $^1\text{J}_{\text{P}-\text{Pt}} = 2325$  Hz) ppm. Anal. Calcd for (C<sub>68</sub>H<sub>76</sub>N<sub>4</sub>P<sub>2</sub>S<sub>2</sub>Pt<sub>2</sub>Zn)<sub>n</sub>: C, 61.14; H, 5.73; N, 4.19. Found: C, 61.34; H, 5.56; N, 4.24. GPC (THF):  $M_w = 112250$ ,  $M_n = 32470$ , PDI = 3.46, DP = 24.

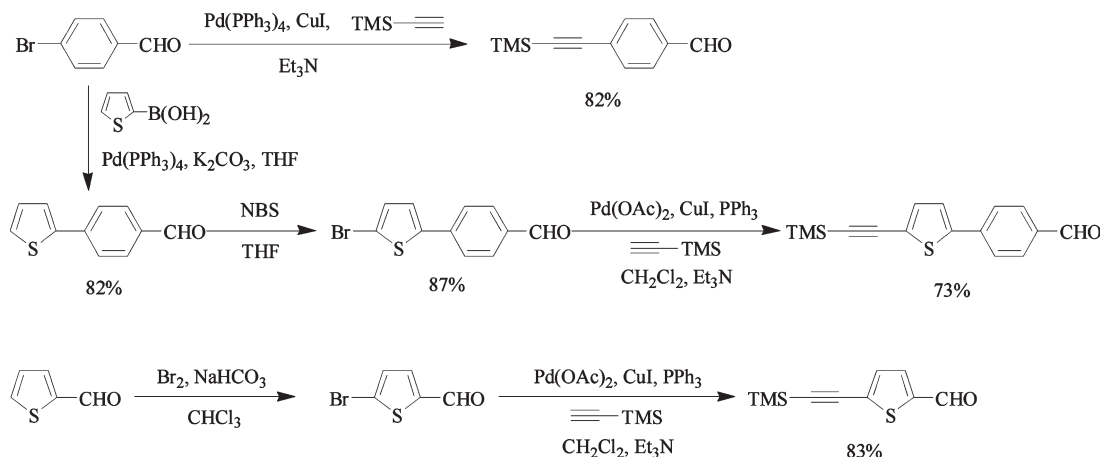
**Synthesis of Platinum Model Complexes (M1–M3).** All of them were synthesized following the dehydrohalogenating coupling between *trans*-[PtCl(Ph)(PEt<sub>3</sub>)<sub>2</sub>] and their corresponding diterminal alkynes. A typical procedure was given for M1 starting from L1.

To a solution of L1 (6 mg, 0.008 mmol) and *trans*-[PtCl(Ph)(PEt<sub>3</sub>)<sub>2</sub>] (10 mg, 0.018 mmol) in Et<sub>3</sub>N (2 mL) and CH<sub>2</sub>Cl<sub>2</sub> (2 mL) was added CuI (1.0 mg) under nitrogen. After stirring overnight at room temperature, all volatile components were removed under reduced pressure. The residue was dissolved in CH<sub>2</sub>Cl<sub>2</sub> and purified by preparative silica TLC plates using CH<sub>2</sub>Cl<sub>2</sub>/hexane as the eluent. The product M1 was obtained as a purple solid (6 mg, 46%).  $\nu(\text{C}\equiv\text{C})$  2091  $\text{cm}^{-1}$ ;  $^1\text{H}$  NMR ( $\text{CDCl}_3$ , 400 MHz,  $\delta$ ): 9.04 (d,  $J = 4.6$  Hz, 4H, Ar), 8.93 (d,  $J = 4.7$  Hz, 4H, Ar), 8.24–8.22 (m, 4H, Ar), 8.05 (d,  $J = 8.1$  Hz, 4H, Ar), 7.79–7.73 (m, 6H, Ar), 7.69–7.67 (m, 4H, Ar), 7.40 (d,  $J = 7.1$  Hz, 4H, Ar), 7.02 (t,  $J = 7.4$  Hz, 4H, Ar), 6.85 (t,  $J = 7.2$  Hz, 2H, Ar), 1.92–1.87 (m, 24H, PEt<sub>3</sub>), 1.25–1.21 (m, 36H, PEt<sub>3</sub>) ppm;  $^{31}\text{P}$  NMR ( $\text{CDCl}_3$ , 162 Hz,  $\delta$ ): 10.08 ( $^1\text{J}_{\text{P}-\text{Pt}} = 2639$  Hz) ppm; FAB-MS:  $m/z$  1739.7 ( $\text{M}^+$ ). Anal. Calcd for C<sub>84</sub>H<sub>96</sub>N<sub>4</sub>P<sub>4</sub>Pt<sub>2</sub>Zn: C, 57.95; H, 5.56; N, 3.22. Found: C, 58.12; H, 5.43; N, 3.45.

**M2.** Purple solid, yield: 38%.  $\nu(\text{C}\equiv\text{C})$  2079  $\text{cm}^{-1}$ .  $^1\text{H}$  NMR ( $\text{CDCl}_3$ , 400 MHz,  $\delta$ ): 9.05–9.03 (m, 4H, Ar), 8.96–8.94 (m, 4H, Ar), 8.22 (d,  $J = 6.5$  Hz, 4H, Ar), 8.18 (d,  $J = 7.7$  Hz, 4H, Ar), 7.93 (d,  $J = 8.1$  Hz, 4H, Ar), 7.79–7.75 (m, 6H, Ar), 7.41 (d,  $J = 3.7$  Hz, 2H, Ar), 7.35 (d,  $J = 7.0$  Hz, 4H, Ar), 7.01–6.97 (m, 6H, Ar), 6.83 (t,  $J = 7.2$  Hz, 2H, Ar), 1.84–1.74 (m, 24H, PEt<sub>3</sub>), 1.25–1.19 (m, 36H, PEt<sub>3</sub>) ppm.  $^{31}\text{P}$  NMR ( $\text{CDCl}_3$ , 162 Hz,  $\delta$ ): 10.01 ( $^1\text{J}_{\text{P}-\text{Pt}} = 2627$  Hz) ppm. MALDI–TOF:  $m/z$  1905.4798 [ $\text{M} + \text{H}]^+$ , calculated: 1904.4922. Anal. Calcd for C<sub>92</sub>H<sub>100</sub>N<sub>4</sub>P<sub>4</sub>S<sub>2</sub>Pt<sub>2</sub>Zn: C, 57.99; H, 5.29; N, 2.94. Found: C, 57.76; H, 5.34; N, 3.20.

**M3.** Purple solid, yield: 48%.  $\nu(\text{C}\equiv\text{C})$  2081  $\text{cm}^{-1}$ .  $^1\text{H}$  NMR ( $\text{CDCl}_3$ , 400 MHz,  $\delta$ ): 9.30 (d,  $J = 4.7$  Hz, 4H, Ar), 8.92 (d,  $J = 4.7$  Hz, 4H, Ar), 8.22–8.19 (m, 4H, Ar), 7.79–7.73 (m, 6H, Ar), 7.64 (d,  $J = 3.5$  Hz, 2H, Ar), 7.36 (d,  $J = 7.0$  Hz, 4H, Ar), 7.27 (d,  $J = 3.5$  Hz, 2H, Ar), 6.99 (t,  $J = 7.4$  Hz, 4H, Ar), 6.83 (t,  $J = 7.2$  Hz, 2H, Ar), 1.87–1.80 (m, 24H, PEt<sub>3</sub>), 1.18–1.12 (m, 36H, PEt<sub>3</sub>) ppm.  $^{31}\text{P}$  NMR ( $\text{CDCl}_3$ , 162 Hz,  $\delta$ ): 10.03 ( $^1\text{J}_{\text{P}-\text{Pt}} = 2630$  Hz) ppm. FAB-MS:  $m/z$  1751.7 ( $\text{M}^+$ ). Anal. Calcd for C<sub>80</sub>H<sub>92</sub>N<sub>4</sub>P<sub>4</sub>S<sub>2</sub>Pt<sub>2</sub>Zn: C, 54.81; H, 5.29; N, 3.20. Found: C, 54.98; H, 5.10; N, 3.12.

**Physical Measurements.** Fast atom bombardment (FAB) mass spectra were recorded on a Finnigan MAT SSQ710 system. NMR spectra were measured in CDCl<sub>3</sub> on a Bruker AVANCE 400 MHz FT-NMR spectrometer using tetramethylsilane as an internal standard for  $^1\text{H}$  and  $^{13}\text{C}$  nuclei or 85% H<sub>3</sub>PO<sub>4</sub> as an external standard for  $^{31}\text{P}$  nucleus. UV-visible spectra were obtained on an HP-8453 diode array spectrophotometer. The solution emission spectra of the compounds were measured on a Photon Technology International (PTI) Fluorescence QuantaMaster Series QM1 spectrophotometer. Thermogravimetric analysis (TGA) measurements were performed on thermal gravimetric analyzer (model Perkin-Elmer TGA-6) under a nitrogen flow at a

**Scheme 1.** Synthetic Routes to Ligand Precursors

heating rate of  $15\text{ }^{\circ}\text{C min}^{-1}$ . The gel permeation chromatography (GPC) measurements were performed on the Agilent 1050 HPLC system with VWD, using THF as eluent and polystyrene standards as calibrants. Electrochemical measurements were carried out on a deoxygenated solution of  $[^n\text{Bu}_4\text{N}]^+\text{PF}_6^-$  (0.1 M) in acetonitrile using a computer-controlled electrochemical workstation, a eDAQ EA161 potentiostat electrochemical interface equipped with a thin film coated indium tin oxide (ITO) covered glass working electrode, a Pt wire as the counter electrode, and a Ag/AgCl (in 3 M KCl) as the reference electrode (at the scan rate of  $100\text{ mV s}^{-1}$ ). Polymer film was prepared by dipping a glass plate in the polymer solution of chlorobenzene and then dried under vacuum, and one side of the glass plate had been casted ITO film beforehand. The onset oxidation and reduction potentials were used to determine the HOMO and LUMO energy levels using the equations  $E_{\text{HOMO}} = [-(E_{\text{onset, ox}} \text{ (vs Ag/AgCl)} - E_{\text{onset (NHE vs Ag/AgCl)}})] - 4.50\text{ eV}$  and  $E_{\text{LUMO}} = [-(E_{\text{onset, red}} \text{ (vs Ag/AgCl)} - E_{\text{onset (NHE vs Ag/AgCl)}})] - 4.50\text{ eV}$ , where the potentials for NHE versus vacuum and NHE versus Ag/AgCl are  $4.50$  and  $-0.22\text{ V}$ , respectively.<sup>33</sup>

**Computational Details.** Calculations were performed with the Gaussian 09<sup>34</sup> program at the Université de Sherbrooke with Mammoth super computer supported by le Réseau Québécois de Calculs de Haute Performances. The DFT<sup>35–38</sup> and TDDFT<sup>39–41</sup> were calculated with the B3LYP<sup>42–44</sup> method. 3-21G\*<sup>45–50</sup> basis sets were used for C, H, S, N and Zn. Polarized VDZ (valence double  $\zeta$ )<sup>51</sup> with SBKJC effective core potentials<sup>52–55</sup> were applied for Pt as well. The predicted phosphorescence wavelengths were obtained by energy differences between the total energy of the triplet and singlet optimized states.<sup>56</sup> The calculated absorption spectra and related molecular orbital (MO) contributions were obtained from the TDDFT/singlets output file and GaussSum 2.1.<sup>57</sup>

**Fabrication and Characterization of Bulk Heterojunction Solar Cells.** The device structure was ITO/poly(3,4-ethylene-dioxythiophene):poly(styrenesulfonate) (PEDOT:PSS)/polymer:PCBM blend/Al. Indium tin oxide (ITO) coated glass substrates ( $10\text{ }\Omega$  per square) were cleaned by sonication in toluene, acetone, ethanol, and deionized water, dried in an oven, and then cleaned with UV ozone for 300 s. As-received PEDOT:PSS solution was passed through the  $0.45\text{ }\mu\text{m}$  filter and spin-coated on patterned ITO substrates at 5000 rpm for 2 min, followed by baking in  $\text{N}_2$  at  $120\text{ }^{\circ}\text{C}$  for 20 min. P1–P3:PCBM (1:4 by weight) active layer was prepared by spin-coating the chlorobenzene solution ( $4\text{ mg mL}^{-1}$  of polymer,  $16\text{ mg mL}^{-1}$  of PCBM) at 1000 rpm for 2 min. The substrates were dried at room temperature under high vacuum ( $10^{-5}$  to  $10^{-6}$  Torr) for 2 h and then stored in a glovebox under Ar atmosphere overnight. An Al electrode (100 nm) was evaporated through a shadow mask to define the

active area of the devices (2 mm diameter circle). All the fabrication procedures (except drying, PEDOT:PSS annealing, and Al deposition) and cell characterization were performed in air. PCE was determined from  $J$ – $V$  curve measurement (using a Keithley 2400 sourcemeter) under white light illumination (at  $100\text{ mW cm}^{-2}$ ). For white light efficiency measurements, an Oriel 66002 solar light simulator with an AM1.5 filter was used. The light intensity was measured by a Molelectron Power Max 500D laser power meter.

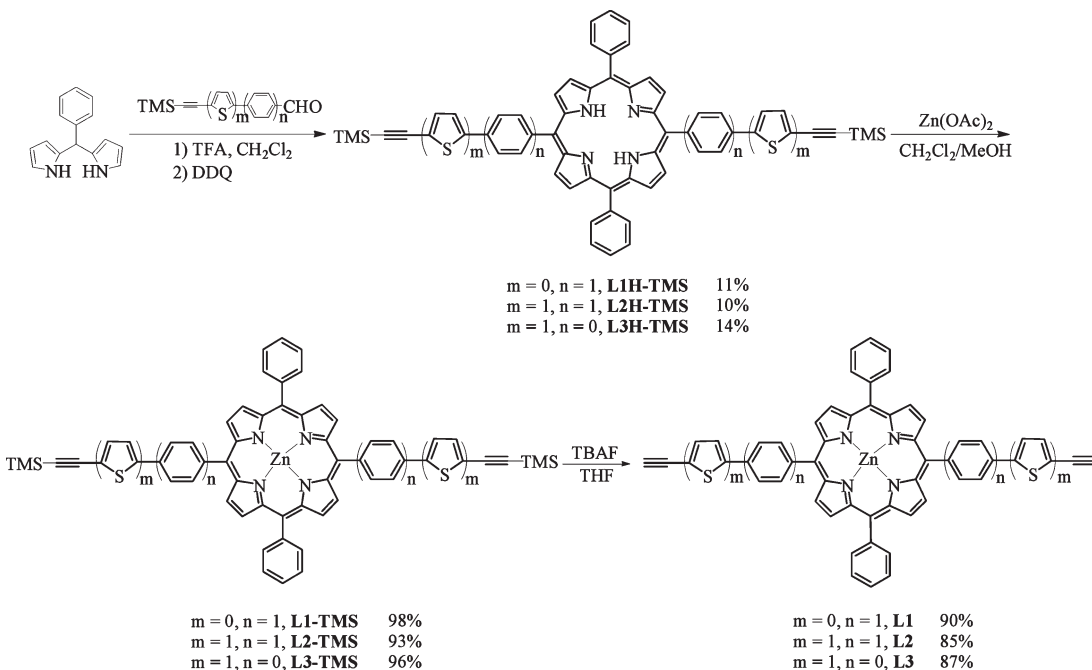
## RESULTS AND DISCUSSION

**Synthesis and Characterization.** The three aromatic aldehyde derivatives were prepared from 4-bromobenzaldehyde and thiophene-2-carbaldehyde according to the pathways depicted in Scheme 1. Following appropriate chemical modifications of the published synthetic procedures, the key *trans*-substituted porphyrins L1H-TMS, L2H-TMS and L3H-TMS were synthesized by the acid-catalyzed condensation of *meso*-phenyldipyrromethane with the aromatic aldehyde derivatives, followed by oxidation with 2,3-dichloro-5,6-dicyano-1,4-benzoquinone (DDQ) at room temperature.<sup>14</sup> The free base porphyrins were then coordinated with zinc(II) ion from zinc acetate in the solvent mixture of  $\text{CH}_2\text{Cl}_2$  and MeOH to form the trimethylsilyl-ethynyl-containing zinc(II) porphyrins L1-TMS to L3-TMS in high yields. The diethynyl ligands L1, L2 and L3 were then prepared by removing the protecting groups with tetrabutylammonium fluoride (TBAF) as shown in Scheme 2.

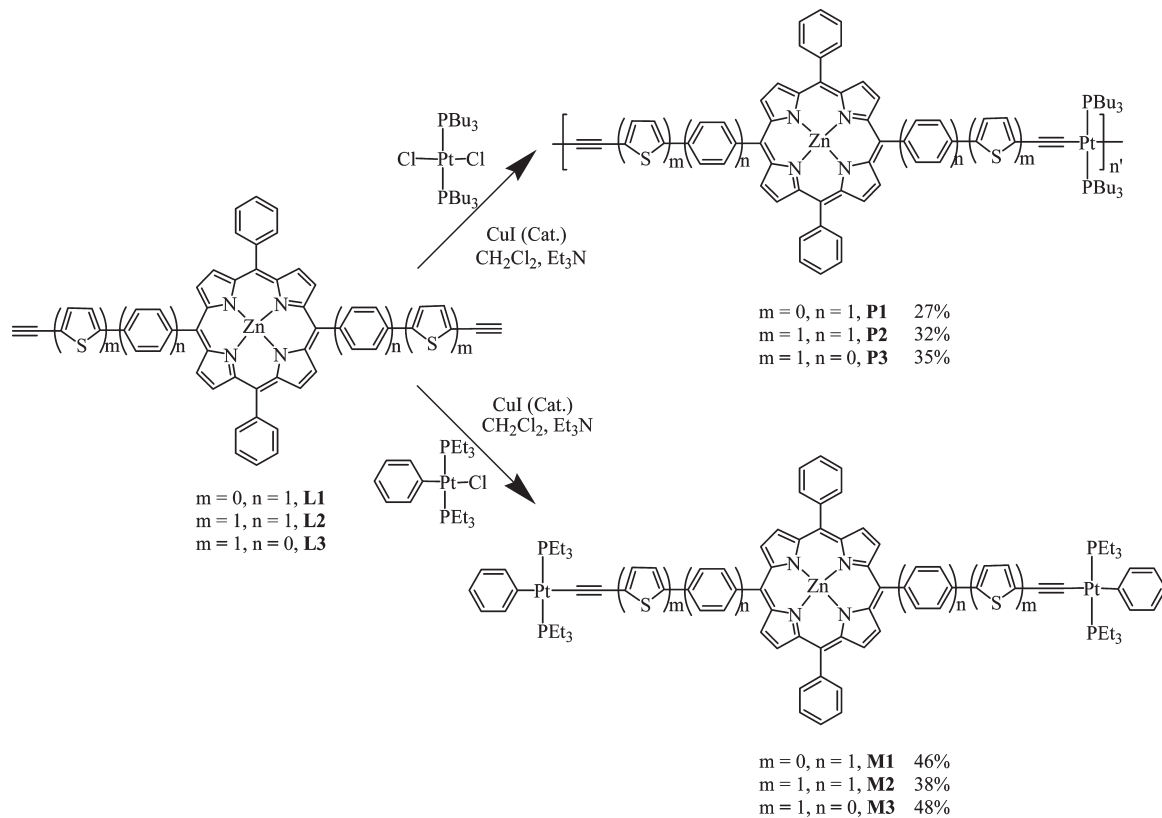
Scheme 3 shows the synthetic routes toward Pt(II)-containing Zn(II)-porphyrinate polymers and their corresponding model complexes. By CuI-catalyzed dehydrohalogenation method, model compounds M1–M3 were prepared from ligands L1–L3 and *trans*-[PtCl(Ph)(PEt<sub>3</sub>)<sub>2</sub>] (in a 1:2.2 stoichiometry) in  $\text{CH}_2\text{Cl}_2$  and Et<sub>3</sub>N (1:1, v/v) in moderate yields. Using the same approach, the reaction of metalloligands with *trans*-[Pt(*n*-Bu<sub>3</sub>P)<sub>2</sub>Cl<sub>2</sub>] in a 1:1 ratio gave the respective polymers P1, P2, and P3 in 27–35% yields. All of the metal alkynyl complexes and polymers are stable and generally exhibit good solubility in chlorocarbons  $\text{CH}_2\text{Cl}_2$  and  $\text{CHCl}_3$ . For P3, it is more soluble in THF and chlorobenzene than in chloroalkanes.

FTIR spectra show that the  $\nu(\text{C}\equiv\text{C})$  stretching frequencies for the platinum polymers at about  $2086\text{ cm}^{-1}$  and model compounds at about  $2081\text{ cm}^{-1}$  are lower than those for the free diethynyl ligands near  $2101\text{ cm}^{-1}$ , which reveal a higher

Scheme 2. Synthetic Pathways to Diethynyl Ligands L1–L3



Scheme 3. Synthetic Pathways to Pt(II) Polyynes P1–P3 and Diynes M1–M3



degree of conjugation in the former. Moreover, the absence of the stretching vibrations for the terminal acetylenic C–H bonds at around  $3286\text{ cm}^{-1}$  further confirms the successful formation

of platinum–carbon bond.  $^{31}\text{P}$  NMR spectra of the platinum-containing complexes and polymers exhibit a strong  $^{31}\text{P}$  singlet signal flanked with two satellites, consistent with a *trans*-geometry

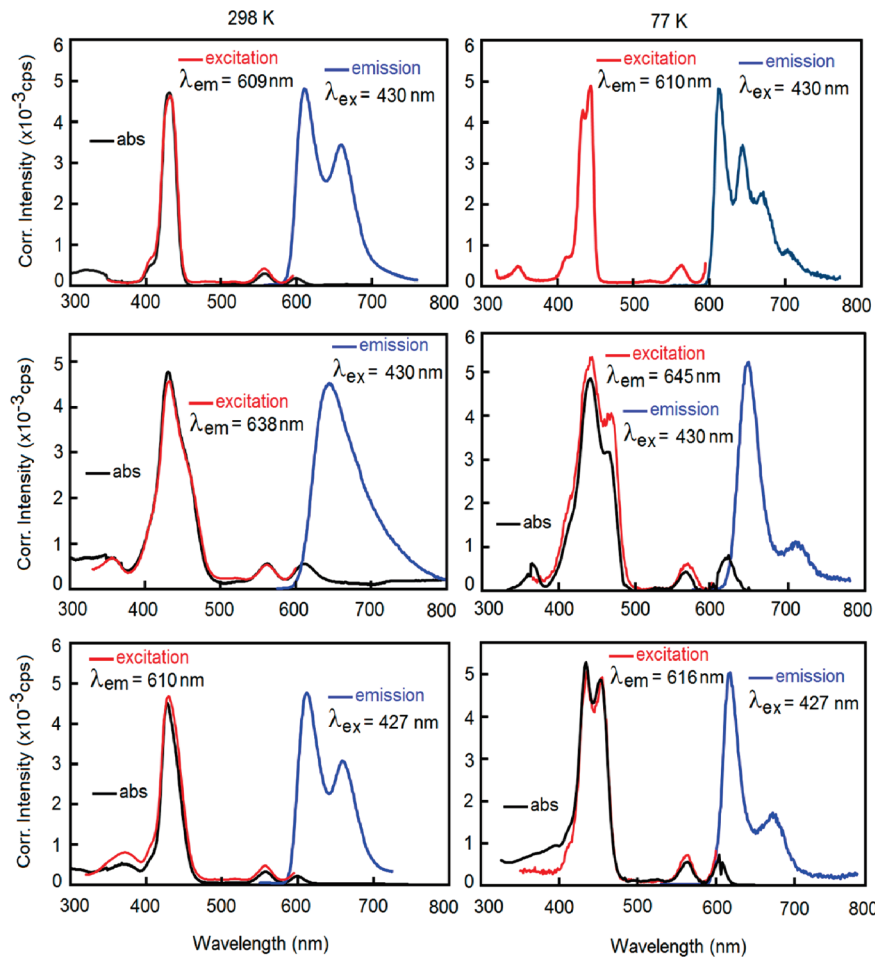


**Figure 1.** Absorption (black), excitation (red) and fluorescence (blue) spectra of P1 (up), P3 (middle), and P2 (bottom) in 2-MeTHF at 298 (left) and 77 K (right).

of the square-planar Pt unit, and their  $^1J_{\text{P}-\text{Pt}}$  values between 2627 to 2639 Hz for the PEt<sub>3</sub> moieties and 2325 and 2352 Hz for the PBu<sub>3</sub> moieties are typical of those for related *trans*-PtP<sub>2</sub> systems.<sup>58</sup> The Pt model complexes were also successfully characterized by mass spectrometry in which the respective molecular ion was observed in each case.

Molecular weights of these polymers were determined by GPC in THF solution using polystyrene standards for the method calibration. P2 has a relatively higher degree of polymerization than that of P1. This is probably ascribed to the more reactive terminal acetylenic C–H bond at the  $\alpha$ -position of thiophene ring than that of benzene ring in the dehydrohalogenative polymerization reaction. This is also corroborated with the data of P3, which has a  $M_n$  of 32470 with a higher degree of polymerization of 24.

The thermal properties of the polymers were determined by thermogravimetric analysis (TGA). The polymers P1, P2, and P3 have relatively good thermal stability with onset decomposition temperatures of 305, 348, and 366 °C, respectively.

**Absorption and Photoluminescence Spectra.** The absorption and emission data for the three polymers are presented in Figure 1 and Table 1. All the polymers show a sharp and strong Soret band at about 430 nm ( $\pi \rightarrow \pi^*$  transition, S<sub>0</sub> → S<sub>2</sub>) and a set of weak Q-bands between 540 and 635 nm ( $\pi \rightarrow \pi^*$  transition, S<sub>0</sub> → S<sub>1</sub>), which is a typical absorption profile for

**Table 1. Spectral (Absorption, Top; Fluorescence, Bottom) and Photophysical Parameters**

polymer in 2-MeTHF				
polymer	temp (K)	Soret, $\lambda$ (nm)	Q-region, $\lambda$ (nm)	
P1	298	398 sh, 430	508 sh, 550, 593	
	77	342	406 sh, 432, 442	522 sh, 558, 598
P3	298	297, 348	434, 456 sh	555, 607
	77	364	438, 460	522, 562, 612
P2	298	377	401, 426	552, 610
	77	382	410, 432, 448	556, 600
298 K				
polymer	$\lambda_F$ (nm)	$\Phi_F$	$\tau_F$ (ns)	$\lambda_F$ (nm)
P1	608, 655	0.081	0.28	612, 642, 663, 699
P3	639	0.029	<0.10	644, 705
P2	609, 655	0.085	0.35	615, 665
77 K				
			$\tau_F$ (ns)	

porphyrin-type compounds.<sup>60</sup> Compared to the absorption features of the corresponding diethynyl ligands, the Soret band and Q-bands of the polymers occur with a slight red-shift of 1–5 nm. This observation illustrates that these polymers do not

exhibit significant  $\pi$ -conjugation because the large aryl–porphyrin dihedral angles, which result from steric interactions with the  $\beta$ -hydrogens, lead to the nonplanarity.<sup>59a</sup> The similar phenomenon takes place in the absorption features of the model complexes (see Supporting Information).

In the photoluminescence spectra, the three polymers exhibit strong luminescence bands between 575 and 790 nm. Since internal conversion is rapid, the photoluminescence seems to occur at the onset positions of their absorption Q-bands.<sup>14,59b</sup> Similarly, the luminescence bands of the polymers undergo a relatively modest red-shift of about 12 nm as compared to that of their corresponding ligands, indicating that the conjugation is moderate.

The excitation spectra superimpose the absorption ones, which indicate that the observed emissions arise from the species generating the absorption spectra (i.e., there are no obvious impurities). The fact that the emission lifetimes are in the short ns time scale and that the energy gap between the lowest energy absorption peak and the highest energy emission signal is relatively small (i.e., notably 10–15 nm for P1 and P2) indicate that the luminescence is indeed fluorescence. Moreover, the very short fluorescence lifetimes,  $\tau_F$ , are consistent with what is generally encountered for low-bandgap Pt-containing polymers.<sup>59c,60</sup> The dinuclear model complexes behave almost the same way as described above for the polymers and no further description is needed for these materials (see Supporting Information).

The comparison between P1 and P3 indicates more red-shifted Soret band and Q-bands by 10–15 nm for the latter, and by 30 nm or so for the emission bands for the latter as well, witnessing the substituent effect of the thiophene residue onto the  $\pi\pi^*$ -type transitions of the zinc(II)-porphyrin unit. This effect may also be ascribed to the better dihedral angle between the average planes for the thiophene versus the metalloporphyrin one in P3, in comparison with the planes between the phenyl versus metalloporphyrin ring in P1. In the absence of X-ray crystal structures, density functional theory (DFT) geometry optimizations were performed instead (vide infra). Indeed, the calculated dihedral angle in P1 (average of 71.5°) is less favorable for conjugation whereas in P3 this angle varies from 64 to 71° (averaging 68.3°). The emission band for the polymer P3 appears broader than that for P1 exhibiting less vibronic structures even at 77 K. This is indicative of low-frequency vibrational modes being Franck–Condon active in the emission band of P3.

One of the surprising features is that the absorption and emission spectra for P2 are not more red-shifted with respect to P1 and P3. In fact, the positions of the peaks are closer to that of P1 for the Soret band and to P3 for the Q-bands (Table 1). The shapes of the emission spectra of P2 are reminiscent of those for P1 at 298 K and P3 at 77 K, indicating that both substituents induce some effects on the luminescent state. The comparison of the photophysical parameters is also presented in Table 1. The striking feature is that both the fluorescence quantum yields,  $\Phi_F$ , and lifetimes,  $\tau_F$ , at 298 and 77 K for polymers P1 and P2 are very similar, whereas those for P3 are very different. Overall, the photophysical features of P2 are more similar to those for the P1 one. The reason for this notable resemblance may come from the polymer structure itself where the immediate substituent around the central zinc(porphyrin) chromophore is the same between P1 and P2 (i.e., a phenyl group attached at the *meso*-position of the zinc(porphyrin) in both cases). Evidence for weak conjugation associated with the large dihedral angle of the *meso*-phenyl and -thiophene substituent is clearly addressed by means of

TDDFT calculations (vide infra). No phosphorescence band was observed in these polymers, even at 77 K. Despite the absence of phosphorescence in P1, P2, and P3, the triplet states are nonetheless populated. In a recent work, a series of polymer closely related to P1 of this work were investigated.<sup>59c</sup> Evidence for  $T_1$  population was made from the measurements of the weak phosphorescence band at 77 K, but also from  $T_1-T_n$  transient absorption spectroscopy. In addition, Schanze and co-workers demonstrated the involvement of the triplet state for energy conversion in solar cells for polymer of the type  $(-C\equiv C-PtL_2-C\equiv C-\text{thiophene}-)_n$  ( $L = PBu_3$ ).<sup>25</sup> They also demonstrated the very rapid intersystem crossing rate constant ( $k_{ISC} \sim 10^{11} \text{ s}^{-1}$ ) in materials containing the fragment  $Ar-C\equiv C-PtL_2-C\equiv C-Ar$  where  $L = PBu_3$  and  $Ar =$  one or many aromatic groups.<sup>19b</sup> So, the triplet state is readily populated, but this is not a guarantee that the materials will be phosphorescent.

**Spectroscopic and Computational Analyses.** The frontier MOs going from HOMO-5 to LUMO+3 are presented in Figures 2–4 for the three polymers. The HOMO, HOMO-1, HOMO-2 and HOMO-3 exhibit atomic contributions of the  $\pi$ -systems spreading from a metalloporphyrin chromophore to one or two Pt-containing spacer  $-Ar-C\equiv C-PtL_2-C\equiv C-Ar-$  ( $Ar = C_6H_4, C_4H_2S, C_6H_4-C_4H_2S; L = PBu_3$ ). This computed feature suggests the presence of conjugation, which is consistent with the substituent effect as discussed above, but also indicates that the conjugation does not spread over a very long segment of the chain, which is consistent with the lack of band shifting between P1 and P2.

The MOs placed at lower energies such as HOMO-4 and HOMO-5 for P1 and P3 exhibit rather localized atomic contributions associated with  $\pi$ -systems centered on a metalloporphyrin chromophore. Similarly, the LUMO, LUMO+1, LUMO+2, and LUMO+3 exhibit atomic contributions pretty much localized onto the zinc(porphyrin) unit. For P3, some minor atomic contributions located on adjacent metalloporphyrins are also computed. All in all, these computations suggest that the excited states are localized on the zinc(porphyrin) unit. This observation is consistent with the strong resemblance between the absorption and fluorescence spectra of the polymers and a single zinc(porphyrin) unit. The exception for P3 may be explained, in part, by the presence of  $\pi$ -system atomic contributions over more than one zinc(porphyrin) unit in the LUMO, LUMO+1, LUMO+2 and LUMO+3 (Figure 3).

TDDFT was employed to address the nature of the lowest  $S_1$  excited states for the three polymers to see whether these correspond to zinc(porphyrin)-localized  $\pi\pi^*$ -type electronic transitions or spacer-to-porphyrin charge transfers as it would simply be suggested by the HOMOs and LUMOs presented in Figures 2–4. Tables 2–4 show the computed electronic transitions along with their positions and oscillator strength (f). The key feature is that the first 4 and 3 electronic transitions for P1 and P2, respectively, are all from lower energy HOMOs and LUMO, LUMO+1, LUMO+2, or LUMO+3. These are all zinc(porphyrin)-localized  $\pi\pi^*$ -type electronic transitions. These common features are consistent with the resemblance in the spectral and photophysical data as discussed above. Conversely, among the 10 lowest energy transitions computed for P3, two are zinc(porphyrin)-localized  $\pi\pi^*$ -type electronic transitions (numbers 1 and 3), and the others are spacer-to-porphyrin charge-transfer in nature. The lowest energy electronic transition is computed at 566 nm and is of zinc(porphyrin)-localized  $\pi\pi^*$ -type. The next transition is placed at 561 nm and is spacer-to-porphyrin

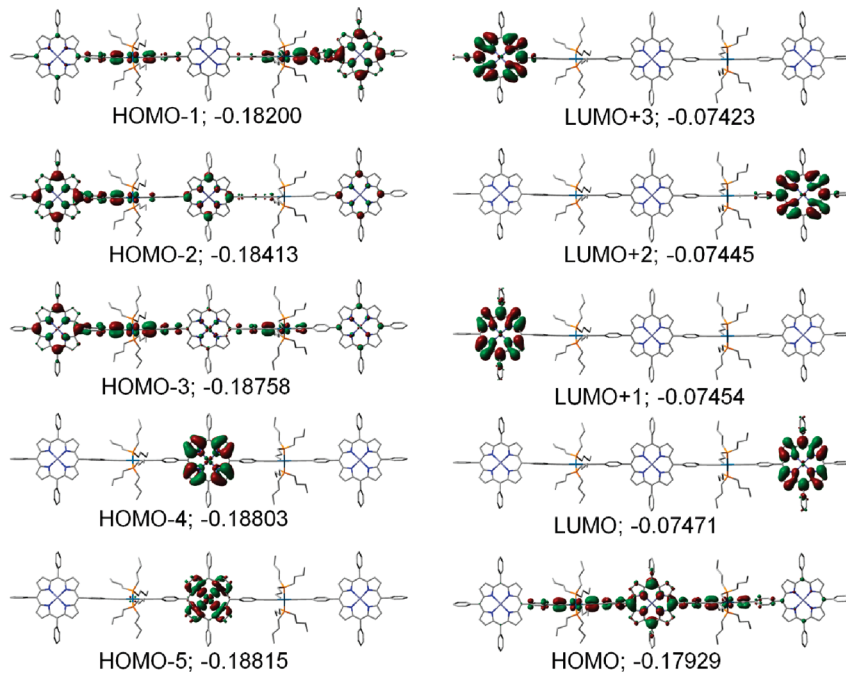


**Figure 2.** Frontier MO representations for an oligomeric model compound of **P1** containing three units.

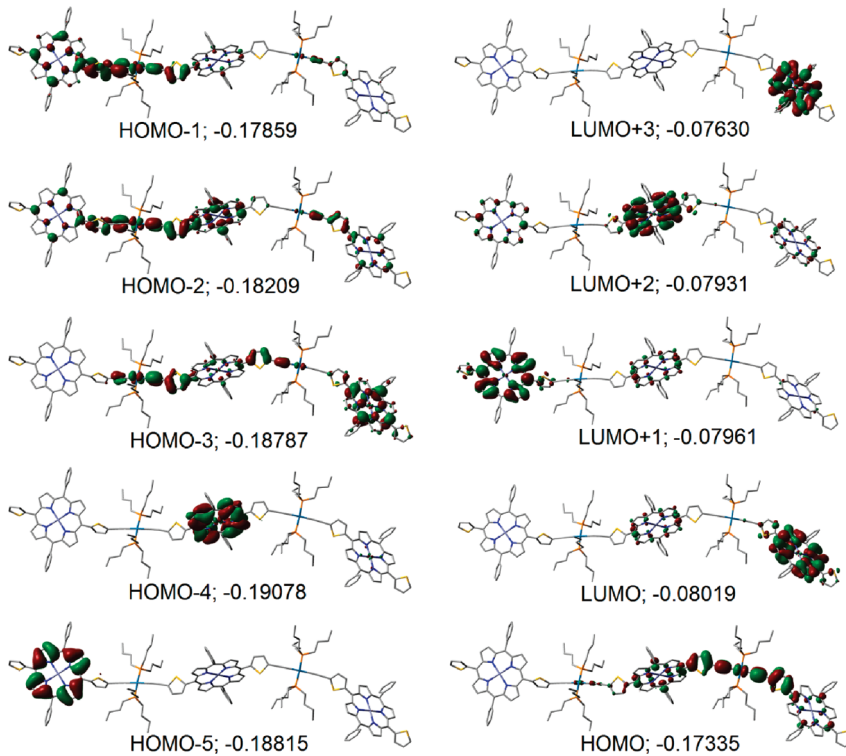


**Figure 3.** Frontier MO representations for an oligomeric model compound of **P3** containing three units.

charge transfer in origin. The close proximity of these two excited states promotes mixing and therefore it would not be surprising to see charge transfer behavior such as that has recently been observed for several polymers and oligomers containing the  $-\text{Ar}-\text{C}\equiv\text{C}-\text{PtL}_2-\text{C}\equiv\text{C}-\text{Ar}-$  spacer ( $\text{Ar} =$  carbazole, quinone diimine).<sup>60–63</sup>

The computed and observed lowest energy peaks are not equal (Table S). There is in fact a difference of an approximate  $1500 \text{ cm}^{-1}$  (i.e., about 45 nm) between the two values. The computed positions of the lowest energy transitions show a blue-shift of about 45 nm; a difference that cannot be accounted for only by the use of gas phase conditions in the calculations.

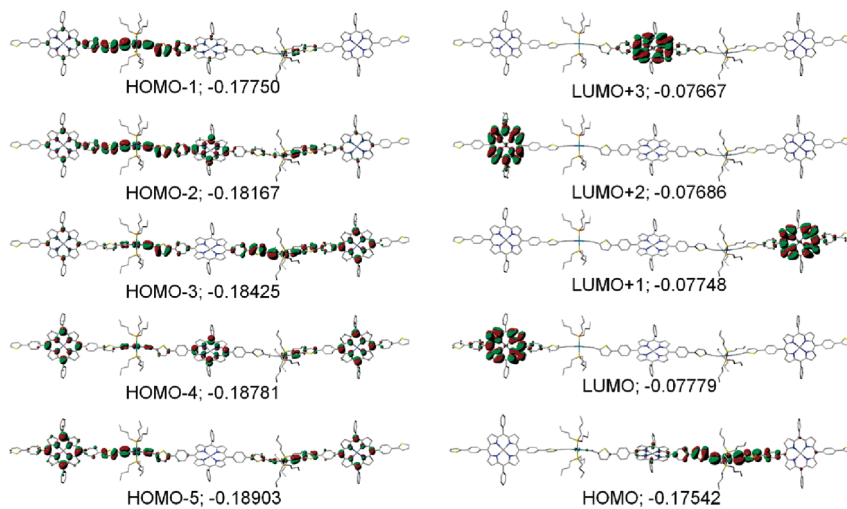


**Figure 4.** Frontier MO representations for an oligomeric model compound of **P2** containing three units.

**Table 2. Computed Positions and Oscillator Strength (*f*) of the 10 Lowest-Energy Electronic Transitions of the Model Compound Used for **P1** as Shown in Figure 2**

no.	$\nu$ (cm <sup>-1</sup> )	$\lambda$ (nm)	<i>f</i>	major contributions (%)
1	18 237	548	0	H-6→L+1 (87), H-5→L+1 (11)
2	18 253	548	0.0001	H-6→LUMO (88)
3	18 369	544	0	H-4→L+2 (97)
4	18 436	542	0	H-4→L+3 (96)
5	19 503	517	0.0132	H-5→LUMO (31), H-1→L+1 (13), HOMO→L+1 (30)
6	19 511	513	0.0605	H-5→L+1 (29), H-1→LUMO (13), HOMO→LUMO (32)
7	19 703	508	0.0069	H-3→L+3 (41), H-1→L+2 (35), HOMO→L+2 (16)
8	19 709	507	0.0181	H-3→L+2 (41), H-1→L+3 (35), HOMO→L+3 (17)
9	21 568	464	0.1044	H-2→L+3 (22), HOMO→L+3 (60)
10	21 720	460	0.0011	H-2→L+2 (21), HOMO→L+2 (68)

**Table 3. Computed Positions and Oscillator Strength (*f*) of the 10 Lowest-Energy Electronic Transitions of the Model Compound Used for **P2** as Shown in Figure 4**

no.	$\nu$ (cm <sup>-1</sup> )	$\lambda$ (nm)	<i>f</i>	major contributions (%)
1	18 077	553	0	H-7→LUMO (31), H-5→LUMO (68)
2	18 122	552	0.0001	H-4→L+1 (96)
3	18 211	549	0	H-7→L+2 (30), H-5→L+2 (70)
4	18 213	549	0	H-4→L+3 (97)
5	19 177	521	0.4474	H-6→L+3 (12), H-1→LUMO (13), H-1→L+1 (11), HOMO→LUMO (19), HOMO→L+1 (20)
6	19 245	520	0.0002	H-7→L+2 (10), H-6→L+3 (13), H-1→LUMO (15), HOMO→LUMO (13), HOMO→L+1 (21)
7	19 328	517	0.0072	H-7→LUMO (25), H-5→LUMO (11), H-1→L+2 (25), HOMO→L+2 (22)
8	19 328	517	0.0092	H-6→L+1 (32), H-2→L+3 (14), H-1→L+3 (18), HOMO→L+3 (31)
9	20 393	490	0.1477	H-3→LUMO (12), H-2→LUMO (10), HOMO→LUMO (43)
10	20 455	489	0.0118	H-6→L+3 (10), H-2→L+1 (19), HOMO→LUMO (13), HOMO→L+1 (40)

Previous works on this type of spacer demonstrated that the difference between gas phase and solvated species is about several nanometers.<sup>64,65</sup>

The computed spectra for the polymers using the model compounds shown in Figures 2–4 are presented in Figure 5. These are generated by computing the first 100 electronic transitions and then a bar graph was generated by plotting the intensity versus the position in nm. Many of these transitions

have no intensity. By assigning a thickness to these transitions, one can generate the computed spectra as depicted in Figure 5.

The calculated absorption spectra (Figure 5) exhibit features as discussed above. First, the positions of the lowest-energy electronic transitions for **P1** and **P2** are almost the same, whereas that for **P3** is more red-shifted. The second striking feature lies in the presence of two well separated peaks in the Soret region of **P2** (red curve in Figure 5). This split is clearly seen in the 77 K spectra of both the **P3**

**Table 4. Computed Positions and Oscillator Strength (*f*) of the 10 Lowest-Energy Electronic Transitions of the Model Compound Used for P3 as Shown in Figure 3**

no.	$\nu$ (cm <sup>-1</sup> )	$\lambda$ (nm)	<i>f</i>	major contributions (%)
1	17 672	566	0.0001	H-6→LUMO (61), H-5→LUMO (26), H-4→LUMO (12)
2	17 829	561	0.0018	H-3→L+1 (95)
3	18 370	544	0.0015	H-6→L+2 (62), H-5→L+2 (24), H-4→L+2 (14)
4	18 450	542	0.4214	H-2→L+3 (10), H-1→LUMO (16), HOMO→LUMO (19), HOMO→L+1 (41)
5	18 464	542	0.0023	H-3→L+3 (94)
6	18 612	537	0.0154	H-1→LUMO (28), HOMO→LUMO (20), HOMO→L+1 (28)
7	18 898	529	0.0095	H-2→L+1 (30), H-1→L+3 (11), HOMO→L+3 (54)
8	18 998	526	0.0059	H-5→LUMO (19), H-4→LUMO (13), H-1→L+2 (37), HOMO→L+2 (23)
9	20 049	499	0.0056	H-4→LUMO (11), H-1→LUMO (13), HOMO→LUMO (47)
10	20 649	484	0.0906	H-7→L+1 (24), H-2→L+3 (14), H-1→LUMO (11), H-1→L+1 (15), HOMO→L+1 (14)

**Table 5. Comparison between the Experimental and Calculated Positions of the Lowest Energy Q-Bands.<sup>a</sup>**

	$\lambda_{\text{abs}}$ (nm)	$\lambda_{\text{abs}}$ (cm <sup>-1</sup> )	$\lambda_{\text{calcd}}$ (nm)	$\lambda_{\text{calcd}}$ (cm <sup>-1</sup> )	$\Delta$ (cm <sup>-1</sup> ) <sup>b</sup>
	77 K	77 K			
P1	598	16 722	548	18 253	1531
P3	612	16 340	566	17 829	1489
P2	600	16 667	552	18 122	1455

<sup>a</sup> The 77 K data are selected for better accuracy. Only calculated data for the gas phase are investigated. Previous experience demonstrated that the incorporation of a solvent has a minor effect (several nm).<sup>64,65</sup> <sup>b</sup>  $\Delta$  is the difference of the calculated and experimental positions in cm<sup>-1</sup>.

and P2 spectra. These splits are due to exciton couplings.<sup>66</sup> The presence of such couplings indicates partial electronic communication that allows the transition moment of the electronic transition to couple with the neighboring ones.

All in all, the TDDFT computations support the  $\pi\pi^*$  assignments localized within the zinc(porphyrin) ring for P1 and P2. In the case of P3, the presence of conjugation is demonstrated and despite the fact that localized  $\pi\pi^*$  transition within the zinc(porphyrin) unit was also observed, some mixing with spacer-to-porphyrin charge transfer character is suspected due to the presence of neighboring transitions placed close in energy, which is consistent with the difference in band-shape of the fluorescence.

No phosphorescence band was observed in this work, even when the time-resolved spectra were measured at 77 K. The calculated positions of the phosphorescence peaks for the model complexes of P1, P2, and P3 are 674.9, 752.8, and 981.1 nm, respectively.

**Electrochemical Properties.** Cyclic voltammetry was employed to determine the oxidation and reduction potentials and qualitatively estimate the highest occupied molecular orbital (HOMO) and the lowest unoccupied molecular orbital (LUMO) energy levels of the metalloporphyrin-containing poly(metal-laynes). Each of the three polymers shows the irreversible oxidation and reductive waves, probably attributable to the presence of the electron-rich porphyrin units.<sup>14</sup> From Table 6, the Pt/Zn mixed-metal polymers have HOMO energy level at  $-5.53$  to  $-5.62$  eV and LUMO energy level at  $-3.64$  to  $-3.73$  eV, the latter of which is more than 0.3 eV higher than that of the PCBM acceptor, indicating that the energy level positions of the donor and acceptor are suitable for charge transfer and separation at the interface between the donor and acceptor.<sup>67</sup> The electrochemical band-gaps between 1.82 and 1.94 eV matched well with their optical

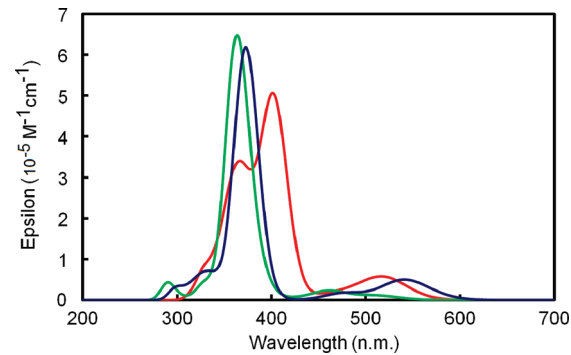


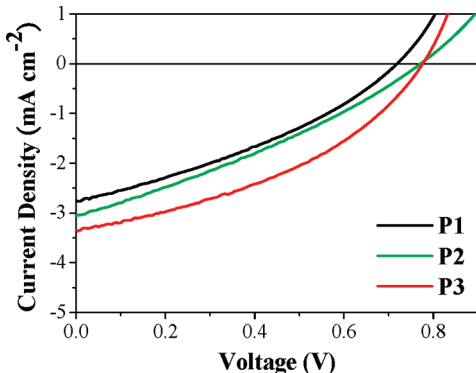
**Figure 5.** Computed spectra of P1 (green), P3 (blue), and P2 (red). Note that no transition was calculated at wavelengths smaller than 290 nm or so. This is due to the limitation in the computed electronic transitions (100).

bandgaps (1.93–2.02 eV) within experimental error, as well as the HOMO–LUMO energy gaps as obtained from the DFT computations above (see Figures 2–4). Compared to P1, polymer P3 has a smaller energy gap because of the stronger electron-donating nature of thiophene than that of benzene, which can increase the energy of the HOMO level and hence decrease the bandgap.<sup>68</sup> From cyclic voltammetry, P2 has the lowest HOMO (close to that for P1) and the lowest LUMO energy levels (close to that for P3), which may be partially attributed to the difficulty in estimating the true potentials for irreversible waves. The relative electrochemical oxidation and reduction peak potentials allow us to state which of the polymers is easier to oxidize and which is easier to reduce. The oxidation peak potentials are P3 ( $+0.81$ )  $<$  P1 ( $+0.86$ )  $<$  P2 ( $+0.90$  V vs Ag/AgCl) indicating that P3 is easier to oxidize, which corroborates the fact that this system exhibits better  $\pi$ -conjugation as discussed above. The DFT computations indicate that the corresponding model for P3 exhibits the highest HOMO level and hence it is also the easiest to oxidize. The reduction peak potentials are P2 ( $-0.99$ )  $\approx$  P3 ( $-1.01$ )  $<$  P1 ( $-1.08$  V vs Ag/AgCl). Meanwhile, the DFT computations indicate that the corresponding model for P3 exhibits the lowest LUMO level of the three computed models, suggesting that P3 is predicted to be the easiest to reduce. Experimentally, both P2 and P3 are the easiest ones to reduce with close LUMO levels as determined by the electrochemical method. Although the relative order for the computed LUMO energies for P2 and P3 and the reduction peak positions appears to be reversed, this can readily be explained by the fact that the

**Table 6.** Electrochemical Onset Potentials and Electronic Energy Levels of the Polymers<sup>a</sup>

polymer	$\lambda_{\text{onset}}$ (nm)	$E_g^{\text{opt}}$ (eV)	$E_{\text{ox}}/E_{\text{HOMO}}$ (V)/(eV)	$E_{\text{red}}/E_{\text{LUMO}}$ (V)/(eV)	$E_g^{\text{ec}}$ (eV)
P1	616	2.02	0.86/−5.58	−1.08/−3.64	1.94
P2	619	2.00	0.90/−5.62	−0.99/−3.73	1.89
P3	643	1.93	0.81/−5.53	−1.01/−3.71	1.82

<sup>a</sup> Onset oxidation potential vs Ag/AgCl ( $E_{\text{ox}}$ ), onset reduction potential vs Ag/AgCl ( $E_{\text{red}}$ ), bandgaps derived from the difference between onset potentials of oxidation and reduction ( $E_g^{\text{ec}}$ ),  $E_{\text{HOMO}} = -(E_{\text{ox}} + 4.72)$  eV,  $E_{\text{LUMO}} = -(E_{\text{red}} + 4.72)$  eV, and the optical bandgap was obtained from the equation  $E_g^{\text{opt}} = 1240/\lambda_{\text{onset}}$ , where  $\lambda_{\text{onset}}$  is the onset value of the absorption spectrum in  $\text{CH}_2\text{Cl}_2$ .

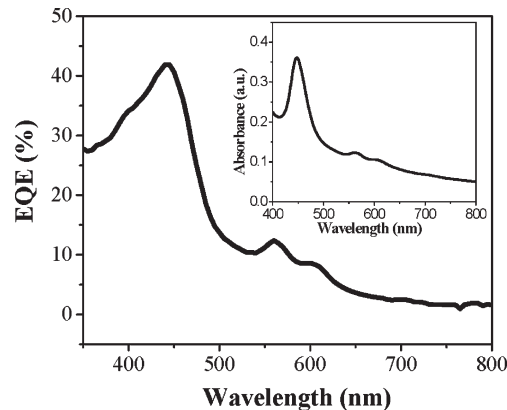
**Figure 6.**  $J$ – $V$  curves of devices based on P1–P3/PCBM blends.

reduction peaks are large and are located at very close values (P2 ( $-0.99$ ) < P3 ( $-1.01$  V vs Ag/AgCl)); i.e. a shift of 0.02 V only) coupled to the fact that gas phase computations and electrochemical measurements in acetonitrile are not ideal for comparison.

**Polymer Photovoltaic Behavior.** Since the light-induced intramolecular electron transfer could easily occur from electron donor to electron acceptor through the  $\pi$ -bridge which favors the photocurrent generation and photoelectronic energy conversion in photovoltaic devices, polymer solar cells were fabricated by using P1, P2, and P3 as the electron donor and PCBM as the electron acceptor with a blend ratio of 1:4. The hole-collection electrode consisted of indium tin oxide (ITO) with a spin-coated poly(3,4-ethylene-dioxythiophene)/poly(styrenesulfonate) (PEDOT/PSS) layer, whereas Al served as the electron-collecting electrode. The current density ( $J$ ) versus voltage ( $V$ ) curves of the solar cells with the blend layer of P1/PCBM, P2/PCBM, and P3/PCBM are displayed in Figure 6. The open-circuit voltage ( $V_{\text{oc}}$ ), short-circuit current density ( $J_{\text{sc}}$ ), fill factor (FF), and PCE of the devices are summarized in Table 7. Polymer P2 shows a relatively larger  $V_{\text{oc}}$  than P1 and P3, consistent with its lowest HOMO energy level, because  $V_{\text{oc}}$  is linearly correlated with the difference of the HOMO of the donor and the LUMO of the acceptor.<sup>69</sup> In the polymer series, P3 exhibited the highest efficiency of 1.04% resulting from the  $V_{\text{oc}}$  of 0.77 V,  $J_{\text{sc}}$  of  $3.42 \text{ mA cm}^{-2}$  and FF of 0.39. This is probably due to its stronger absorption features with a broader Soret band and stronger Q-bands. Such PCE of over 1% is among the highest for bulk heterojunction solar cells based on porphyrin-containing conjugated polymers to date in the literature. In all diodes, FFs are not very impressive, partly because all processing (except PEDOT:PSS annealing and electrode deposition) and measurements have been done under ambient atmosphere, which likely results in the presence of traps. We expect FF to improve for fabrication and characterization to be performed in an inert gas environment. Additional possible reason for the relatively low fill

**Table 7.** Photovoltaic Performance of Metallocporphyrin-Containing Polyplatinynes

polymer/PCBM	$V_{\text{oc}}$ (V)	$J_{\text{sc}}$ ( $\text{mA cm}^{-2}$ )	FF	PCE (%)
P1 (1:4)	0.72	2.74	0.34	0.68
P2 (1:4)	0.78	3.02	0.30	0.71
P3 (1:4)	0.77	3.42	0.39	1.04

**Figure 7.** External quantum efficiency (EQE) versus wavelength curve for the solar cell based on a P2/PCBM blend. The inset shows the absorption spectrum of the polymer blend.

factor include unbalanced charge transport for electrons and holes,<sup>70,71</sup> which cannot be entirely excluded. Comprehensive study of charge transport and the influence of traps is necessary to further improve FF and overall device performance.

The absorption curve of the blend films and external quantum efficiency (EQE) curves of the solar cells based on these Pt/Zn-based polymers and PCBM were also studied for P1 and P2 (Figure 7). For instance, the P1 photodiode shows three main EQE peaks, which correspond to the peaks in the absorption spectrum of the polymer. The absorption is enhanced in the high-energy absorption range 350–415 nm after blending with 80% PCBM. Moreover, the shape of the EQE curve is similar to that of the absorption curve, illustrating that all the light energy absorbed by the polymer/PCBM blend film is to some extent converted into electricity. The excitons produced by absorption in the polymer are dissociated into charge carriers at the contact between polymer and PCBM in the active layer, and are subsequently collected at the electrodes. The highest EQE values of P1 and P2 are 42.4% at 443 nm. The absorption bands of these polymers at 448 nm are narrow, and the Q-bands of porphyrin are still weak in the film absorption spectra. Therefore, the photovoltaic efficiency should be increased by improving the absorption property of porphyrin-containing polymers in the visible region, such as broadening and

enhancing the Q-bands or covering the missing region (430–530 nm) by using perylenetetracarboxylic diimide residues, which should give rise to a strong absorption band between 450 and 600 nm. This is the subject of future attention.<sup>72</sup>

## CONCLUDING REMARKS

A series of soluble platinum metallocopolynes containing Zn-(porphyrin) chromophores and electron-rich aromatic rings (benzene and/or thiophene) were synthesized and systematically characterized. These polymers exhibit a sharp and strong Soret band near 430 nm and two weak Q-bands between 540 and 635 nm, which is a typical absorption profile for porphyrinate compounds. The optical bandgaps for these polymers vary from 1.93 to 2.02 eV, consistent with the electrochemical data. The best photovoltaic performance of devices based on the P3/PCBM blend layer, with  $V_{oc} = 0.77$  eV,  $J_{sc} = 3.42$  mA cm<sup>-2</sup>, FF = 0.39, and PCE = 1.04%, represents the highest value reported so far for bulk heterojunction solar cells based on the porphyrin-containing metallocopolymers. P2 has a lower  $E_g$  than P1 which favors harvesting of more solar photon energy. These deeply colored absorbing polymers are thus attractive candidates as a new class of functional material toward organometallic photovoltaic technology. However, we need more efforts to improve the photon-to-electricity conversion efficiency further for practical applications. One of the major limiting parameters is presumably due to the restricted absorption properties in the visible region. Therefore, it is expected that a continuous optimization of the chemical structures of porphyrin and polymer main chain by incorporating some special functional chromophores would improve the absorption properties and hence enhance the photovoltaic efficiency of porphyrin-containing polymers. The answer to this question probably lies in the design of polymers where more conjugation in the  $\pi$ -system is promoted such as the incorporation of 1,3,4-oxadiazole (Ox) in the spacer (i.e.,  $(-\text{Ox}-\text{C}\equiv\text{C}-\text{PtL}_2-\text{C}\equiv\text{C}-\text{Ox}-\text{metalloporphyrin}-)_n$ ). Such an electron rich aromatic group does not exhibit any C–H bond which can be sterically hindered with the  $\beta$ -proton of the porphyrin, consequently promoting a rather planar arrangement.<sup>73</sup>

## ASSOCIATED CONTENT

**S Supporting Information.** Synthetic procedures and spectroscopic data for some ligand precursors, absorption and emission spectra for L1–L3, M1–M3, and P1–P3 as well as their photoophysical data in THF, and EQE versus wavelength curve for P1. This material is available free of charge via the Internet at <http://pubs.acs.org>.

## AUTHOR INFORMATION

### Corresponding Author

\*Corresponding authors. E-mail: (W.-Y.W.) [rwywong@hkbu.edu.hk](mailto:rwywong@hkbu.edu.hk); (P.D.H.) [Pierre.Harvey@USherbrooke.ca](mailto:Pierre.Harvey@USherbrooke.ca); (A.B.D.) [dalek@hku.hk](mailto:dalek@hku.hk).

## ACKNOWLEDGMENT

W.-Y.W. acknowledges the support from the Hong Kong Research Grants Council for the General Research Grant (Grant no: HKBU 202607) and the Collaborative Research Fund (HKUST2/CRF/10), Hong Kong Baptist University for the FRG grant (FRG2/09-10/091) and the Croucher Foundation for the Croucher Senior Research Fellowship. This work was

also supported by the Areas of Excellence Scheme, University Grants Committee, Hong Kong (AoE/P-03/08). We also thank the Natural Sciences and Engineering Research Council of Canada (NSERC), le Fonds Québécois de la Recherche sur la Nature et les Technologies (FQRNT), and the Centre d'Études des Matériaux Optiques et Photoniques de l'Université de Sherbrooke. This work was also supported by Small Project Funding, Strategic Research Theme, and University Development Fund of the University of Hong Kong.

## REFERENCES

- (1) Sariciftci, N. S.; Smilowitz, L.; Heeger, A. J.; Wudl, F. *Science* **1992**, *258*, 1474–1476.
- (2) Fukuzumi, S.; Endo, Y.; Imahori, H. *J. Am. Chem. Soc.* **2002**, *124*, 10974–10975.
- (3) Hasobe, T.; Imahori, H.; Kamat, P. V.; Ahn, T. K.; Kim, S. K.; Kim, D.; Fujimoto, A.; Hirakawa, T.; Fukuzumi, S. *J. Am. Chem. Soc.* **2005**, *127*, 1216–1228.
- (4) Sun, Q. J.; Dai, L. M.; Zhou, X. L.; Li, L. F.; Li, Q. *Appl. Phys. Lett.* **2007**, *91*, 253505–1–3.
- (5) Hasobe, T.; Sandanayaka, A. S. D.; Wada, T.; Araki, Y. *Chem. Commun.* **2008**, 3372–3374.
- (6) Xiao, S. Q.; Li, Y. L.; Li, Y. J.; Zhuang, J. P.; Wang, N.; Liu, H. B.; Ning, B.; Liu, Y.; Lu, F. S.; Fan, L. Z.; Yang, C. H.; Li, Y. F.; Zhu, D. B. *J. Phys. Chem. B* **2004**, *108*, 16677–16685.
- (7) Lu, F. S.; Xiao, S. Q.; Li, Y. L.; Liu, H. B.; Li, H. M.; Zhuang, J. P.; Liu, Y.; Wang, N.; He, X. R.; Li, X. F.; Gan, L. B.; Zhu, D. B. *Macromolecules* **2004**, *37*, 7444–7450.
- (8) Liu, Y.; Wang, N.; Li, Y. J.; Liu, H. B.; Li, Y. L.; Xiao, J. C.; Xu, X. H.; Huang, C. S.; Cui, S.; Zhu, D. B. *Macromolecules* **2005**, *38*, 4880–4887.
- (9) Walter, M. G.; Rudine, A. B.; Wamser, C. C. *J. Porphyrins Phthalocyanines* **2010**, *14*, 759–792.
- (10) Hasobe, T.; Kamat, P. V.; Absalom, M. A.; Kashiwagi, Y.; Sly, J.; Crossley, M. J.; Hosomizu, K.; Imahori, H.; Fukuzumi, S. *J. Phys. Chem. B* **2004**, *108*, 12865–12872.
- (11) Oku, T.; Noma, T.; Suzuki, A.; Kikuchi, K.; Kikuchi, S. *J. Phys. Chem. Solids* **2010**, *71*, 551–555.
- (12) Hagemann, O.; Jorgensen, M.; Krebs, F. C. *J. Org. Chem.* **2006**, *71*, 5546–5559.
- (13) Krebs, F. C.; Hagemann, O.; Jorgensen, M. *Sol. Energ. Mater. Sol. Cells* **2004**, *83*, 211–228.
- (14) (a) Huang, X. B.; Zhu, C. L.; Zhang, S. M.; Li, W. W.; Guo, Y. L.; Zhan, X. W.; Liu, Y. Q.; Bo, Z. S. *Macromolecules* **2008**, *41*, 6895–6902. (b) Liu, Y.; Guo, X.; Xiang, N.; Zhao, B.; Huang, H.; Li, H.; Shen, P.; Tan, S. *J. Mater. Chem.* **2010**, *20*, 1140–1146. (c) Xiang, N.; Liu, Y.; Zhou, W.; Huang, H.; Guo, X.; Tan, Z.; Zhao, B.; Shen, P.; Tan, S. *Eur. Polym. J.* **2010**, *46*, 1084–1092. (d) Ravikanth, M.; Strachan, J.-P.; Li, F.; Lindsey, J. S. *Tetrahedron* **1998**, *54*, 7721–7734. (e) Liu, Z.; Schmidt, I.; Thamyongkit, P.; Loewe, R. S.; Syomin, D.; Diers, J. R.; Zhao, Q.; Misra, V.; Lindsey, J. S.; Bocian, D. F. *Chem. Mater.* **2005**, *17*, 3728–3742. (f) Rochford, J.; Botchway, S.; McGarvey, J. J.; Rooney, A. D.; Pryce, M. T. *J. Phys. Chem. A* **2008**, *112*, 11611–11618.
- (15) Feng, J.; Zhang, Q.; Li, W.; Li, Y.; Yang, M.; Cao, Y. *J. Appl. Polym. Sci.* **2008**, *109*, 2283–2290.
- (16) Hasobe, T.; Saito, K.; Kamat, P. V.; Troiani, V.; Qiu, H.; Solladié, N.; Kim, K. S.; Park, J. K.; Kim, D.; D'Souza, F.; Fukuzumi, S. *J. Mater. Chem.* **2007**, *17*, 4160–4170.
- (17) Masai, H.; Sonogashira, K.; Hagiwara, N. *Bull. Chem. Soc. Jpn.* **1971**, *44*, 2226–2230.
- (18) Wittmann, H. F.; Fuhrmann, K.; Friend, R. H.; Khan, M. S.; Lewis, J. *Synth. Met.* **1993**, *55*, 56–61.
- (19) (a) Lewis, J.; Khan, M. S.; Johnson, B. F. G.; Marder, T. B.; Fyfe, H. B.; Wittmann, H. F.; Friend, R. H.; Dray, A. E. *J. Organomet. Chem.* **1992**, *425*, 165–176. (b) Rogers, J. E.; Slagle, J. E.; Krein, D. M.; Burke, A. R.; Hall, B. C.; Fratini, A.; McLean, D. G.; Fleitz, P. A.; Cooper, T. M.;

- Drobizhev, M.; Makarov, N. S.; Rebane, A.; Kim, K.-Y.; Farley, R.; Schanze, K. S. *Inorg. Chem.* **2007**, *46*, 6483–6494.
- (20) Wilson, J. S.; Chawdhury, N.; Al-Mandhary, M. R. A.; Younus, M.; Khan, M. S.; Raithby, P. R.; Köhler, A.; Friend, R. H. *J. Am. Chem. Soc.* **2001**, *123*, 9412–9417.
- (21) Wong, W.-Y.; Ho, C. L. *Coord. Chem. Rev.* **2006**, *250*, 2627–2690.
- (22) Wong, W.-Y. *Dalton Trans.* **2007**, 4495–4510.
- (23) Wong, W.-Y.; Harvey, P. D. *Macromol. Rapid Commun.* **2010**, *31*, 671–713.
- (24) Kohler, A.; Wittmann, H. F.; Friend, R. H.; Khan, M. S.; Lewis, J. *Synth. Met.* **1994**, *67*, 245–249.
- (25) Guo, F.; Kim, Y.-G.; Reynolds, J. R.; Schanze, K. S. *Chem. Commun.* **2006**, 1887–1889.
- (26) Wong, W.-Y.; Wang, X. Z.; He, Z.; Chan, K. K.; Djurišić, A. B.; Cheung, K. Y.; Yip, C. T.; Ng, A. M. C.; Xi, Y. Y.; Mak, C. S. K.; Chan, W. K. *J. Am. Chem. Soc.* **2007**, *129*, 14372–14380.
- (27) Wong, W.-Y.; Wang, X. Z.; He, Z.; Djurišić, A. B.; Yip, C. T.; Cheung, K. Y.; Wang, H.; Mak, C. S. K.; Chan, W. K. *Nat. Mater.* **2007**, *6*, 521–527.
- (28) Baek, N. S.; Hau, S. K.; Yip, H.-L.; Acton, O.; Chen, K.-S.; Jen, A. K.-Y. *Chem. Mater.* **2008**, *20*, 5734–5736.
- (29) Yang, F.; Xu, X. L.; Gong, Y. H.; Qiu, W. W.; Sun, Z. R.; Zhou, J. W.; Audebert, P.; Tang, J. *Tetrahedron* **2007**, *63*, 9188–9194.
- (30) Lee, C. H.; Lindsey, J. S. *Tetrahedron* **1994**, *50*, 11427–11440.
- (31) Chatt, J.; Shaw, B. L. *J. Chem. Soc.* **1959**, 4020–4033.
- (32) Kauffman, G. B.; Teter, L. A. *Inorg. Synth.* **1963**, *7*, 245–249.
- (33) Hou, J.; Tan, Z.; Yan, Y.; He, Y.; Yang, C.; Li, Y. *J. Am. Chem. Soc.* **2006**, *128*, 4911–4916.
- (34) Frisch, M. J.; Trucks, G. W.; Schlegel, H. B.; Scuseria, G. E.; Robb, M. A.; Cheeseman, J. R.; Zakrzewski, V. G.; Montgomery, J. A., Jr.; Stratmann, R. E.; Burant, J. C.; Dapprich, S.; Millam, J. M.; Daniels, A. D.; Kudin, K. N.; Strain, M. C.; Farkas, O.; Tomasi, J.; Barone, V.; Cossi, M.; Cammi, R.; Mennucci, B.; Pomelli, C.; Adamo, C.; Clifford, S.; Ochterski, J.; Petersson, G. A.; Ayala, P. Y.; Cui, Q.; Morokuma, K.; Malick, D. K.; Rabuck, A. D.; Raghavachari, K.; Foresman, J. B.; Cioslowski, J.; Ortiz, J. V.; Baboul, A. G.; Stefanov, B. B.; Liu, G.; Liashenko, A.; Piskorz, P.; Komaromi, I.; Gomperts, R.; Martin, R. L.; Fox, D. J.; Keith, T.; Al-Laham, M. A.; Peng, C. Y.; Nanayakkara, A.; Gonzalez, C.; Challacombe, M.; Gill, P. M. W.; Johnson, B. G.; Chen, W.; Wong, M. W.; Andres, J. L.; Head-Gordon, M.; Replogle, E. S.; Pople, J. A. Gaussian 03, revision C.02; Gaussian, Inc.: Pittsburgh PA, 1998 (Gaussian 03, revision C.02).
- (35) Hohenberg, P.; Kohn, W. *Phys. Rev.* **1964**, *136*, B864–871.
- (36) Kohn, W.; Sham, L. *J. Phys. Rev.* **1965**, *140*, A1133–1138.
- (37) Salahub, D. R.; Zerner, M. C. *The Challenge of d and f Electrons*; American Chemical Society: Washington, DC, 1989.
- (38) Parr, R. G.; Yang, W. *Density-Functional Theory of Atoms and Molecules*; Oxford University Press: Oxford, U.K., 1989.
- (39) Stratmann, R. E.; Scuseria, G. E.; Frisch, M. J. *J. Chem. Phys.* **1998**, *109*, 8218–8224.
- (40) Bauernschmitt, R.; Ahlrichs, R. *Chem. Phys. Lett.* **1996**, *256*, 454–464.
- (41) Casida, M. E.; Jamorski, C.; Casida, K. C.; Salahub, D. R. *J. Chem. Phys.* **1998**, *108*, 4439–4449.
- (42) Becke, A. D. *J. Chem. Phys.* **1993**, *98*, 5648–5652.
- (43) Lee, C.; Yang, W.; Parr, R. G. *Phys. Rev. B* **1988**, *37*, 785–789.
- (44) Miehlich, S. A.; Stoll, H.; Preuss, H. *Chem. Phys. Lett.* **1989**, *157*, 200–206.
- (45) Binkley, J. S.; Pople, J. A.; Hehre, W. J. *J. Am. Chem. Soc.* **1980**, *102*, 939–947.
- (46) Gordon, M. S.; Binkley, J. S.; Pople, J. A.; Pietro, W. J.; Hehre, W. J. *J. Am. Chem. Soc.* **1982**, *104*, 2797–2803.
- (47) Pietro, W. J.; Francl, M. M.; Hehre, W. J.; Defrees, D. J.; Pople, J. A.; Binkley, J. S. *J. Am. Chem. Soc.* **1982**, *104*, 5039–5048.
- (48) Dobbs, K. D.; Hehre, W. J. *J. Comput. Chem.* **1986**, *7*, 359–378.
- (49) Dobbs, K. D.; Hehre, W. J. *J. Comput. Chem.* **1987**, *8*, 861–879.
- (50) Dobbs, K. D.; Hehre, W. J. *J. Comput. Chem.* **1987**, *8*, 880–893.
- (51) Weigend, F.; Ahlrichs, R. *Phys. Chem. Chem. Phys.* **2005**, *7*, 3297–3305.
- (52) He, H.; Binkley, J. S.; Pople, J. A.; Hehre, W. J. *J. Am. Chem. Soc.* **1980**, *102*, 939–947.
- (53) Stevens, W. J.; Basch, H.; Krauss, M. *J. Chem. Phys.* **1984**, *81*, 6026–6033.
- (54) Stevens, W. J.; Krauss, M.; Basch, H.; Jasien, P. G. *Can. J. Chem.* **1992**, *70*, 612–630.
- (55) Cundari, T. R.; Stevens, W. J. *J. Chem. Phys.* **1993**, *98*, 5555–5565.
- (56) Lowry, M. S.; Hudson, W. R.; Pascal, R. A., Jr.; Bernhard, S. *J. Am. Chem. Soc.* **2004**, *126*, 14129–14135.
- (57) O'Boyle, N. M.; Tenderholt, A. L.; Langner, K. M. *J. Comput. Chem.* **2008**, *29*, 839–845.
- (58) Chawdhury, N.; Kohler, A.; Friend, R. H.; Wong, W.-Y.; Lewis, J.; Younus, M.; Raithby, P. R.; Corcoran, T. C.; Al-Mandhary, M. R. A.; Khan, M. S. *J. Chem. Phys.* **1999**, *110*, 4963–4970.
- (59) (a) Anderson, H. L. *Chem. Commun.* **1999**, 2323–2330. (b) Yamamoto, T.; Fukushima, N.; Nakajima, H.; Maruyama, T.; Yamaguchi, I. *Macromolecules* **2000**, *33*, 5988–5994. (c) Liu, L.; Fortin, D.; Harvey, P. D. *Inorg. Chem.* **2009**, *48*, 5891–5900.
- (60) Jiang, F. L.; Fortin, D.; Harvey, P. D. *Inorg. Chem.* **2010**, *49*, 2614–2623.
- (61) Aly, S. M.; Ho, C.-L.; Wong, W.-Y.; Abd-El-Aziz, A. S.; Harvey, P. D. *Chem.—Eur. J.* **2008**, *14*, 8341–8352.
- (62) Fortin, D.; Clément, S.; Gagnon, K.; Bérubé, J. F.; Harvey, P. D. *Inorg. Chem.* **2009**, *48*, 446–454.
- (63) Aly, S. M.; Ho, C.-L.; Wong, W.-Y.; Fortin, D.; Harvey, P. D. *Macromolecules* **2009**, *42*, 6902–6916.
- (64) Bellows, D.; Aly, S. M.; Goudreault, T.; Fortin, D.; Gros, C. P.; Barbe, J. M.; Harvey, P. D. *Organometallics* **2010**, *29*, 317–325.
- (65) Gagnon, K.; Bérubé, J. F.; Bellows, D.; Caron, L.; Aly, S. M.; Wittmeyer, A.; Abd-El-Aziz, A. S.; Fortin, D.; Harvey, P. D. *Organometallics* **2008**, *27*, 2201–2214.
- (66) Harvey, P. D. Recent Advances in Free and Metalated Multi-Porphyrin Assemblies and Arrays; A Photophysical Behavior and Energy Transfer Perspective. Invited contribution for *The 2nd Handbook on Porphyrins and Phthalocyanines*; Kadish, K.; Guilard, R.; Smith, K. M., Eds.; Elsevier: Amsterdam, 2003, Chapter 113, pp 63–249.
- (67) Halls, J. J. M.; Cornill, J.; dos Santos, D. A.; Silbey, R.; Hwang, D. H.; Holmes, A. B.; Brédas, J. L.; Friend, R. H. *Phys. Rev. B* **1999**, *60*, 5721–5727.
- (68) Kanimozhhi, C.; Balraju, P.; Sharma, G. D.; Patil, S. *J. Phys. Chem. B* **2010**, *114*, 3095–3103.
- (69) Scharber, M. C.; Mühlbacher, D.; Koppe, M.; Denk, P.; Waldauf, C.; Heeger, A. J.; Brabec, C. J. *Adv. Mater.* **2006**, *18*, 789–794.
- (70) Kotlarski, J. D.; Moet, D. J. D.; Blom, P. W. M. *J. Polym. Sci., Part B: Polym. Phys.* **2011**, *49*, 708–711.
- (71) Fabiano, S.; Chen, Z.; Vahedi, S.; Facchetti, A.; Pignataro, B.; Loi, M. A. *J. Mater. Chem.* **2011**, *21*, 5891–5896.
- (72) (a) Xue, C. M.; Chen, M. Z.; Jin, S. *Polymer* **2008**, *49*, 5314–5321. (b) Zhang, R. L.; Wu, Y. S.; Wang, Z. L.; Xue, W.; Fu, H. B.; Yao, J. N. *J. Phys. Chem. C* **2009**, *113*, 2594–2602. (c) Wang, D. L.; Shi, Y.; Zhao, C. T.; Liang, B. L.; Li, X. Y. *J. Mol. Struct.* **2009**, *938*, 245–253. (d) Koyuncu, S.; Zafer, C.; Koyuncu, F. B.; Aydin, B.; Can, M.; Sefer, E.; Ozdemir, E.; Icli, S. *J. Polym. Sci. A: Polym. Chem.* **2009**, *47*, 6280–6291. (e) Wang, Y. F.; Chen, H. L.; Wu, H. X.; Li, X. Y.; Weng, Y. X. *J. Am. Chem. Soc.* **2009**, *131*, 30–31.
- (73) Goudreault, T.; He, Z.; Guo, Y. H.; Ho, C.-L.; Wang, Q. W.; Zhan, H. M.; Wong, K. L.; Fortin, D.; Yao, B.; Xie, Z. Y.; Kwok, W.-M.; Wong, W.-Y.; Harvey, P. D. *Macromolecules* **2010**, *43*, 7936–7949.